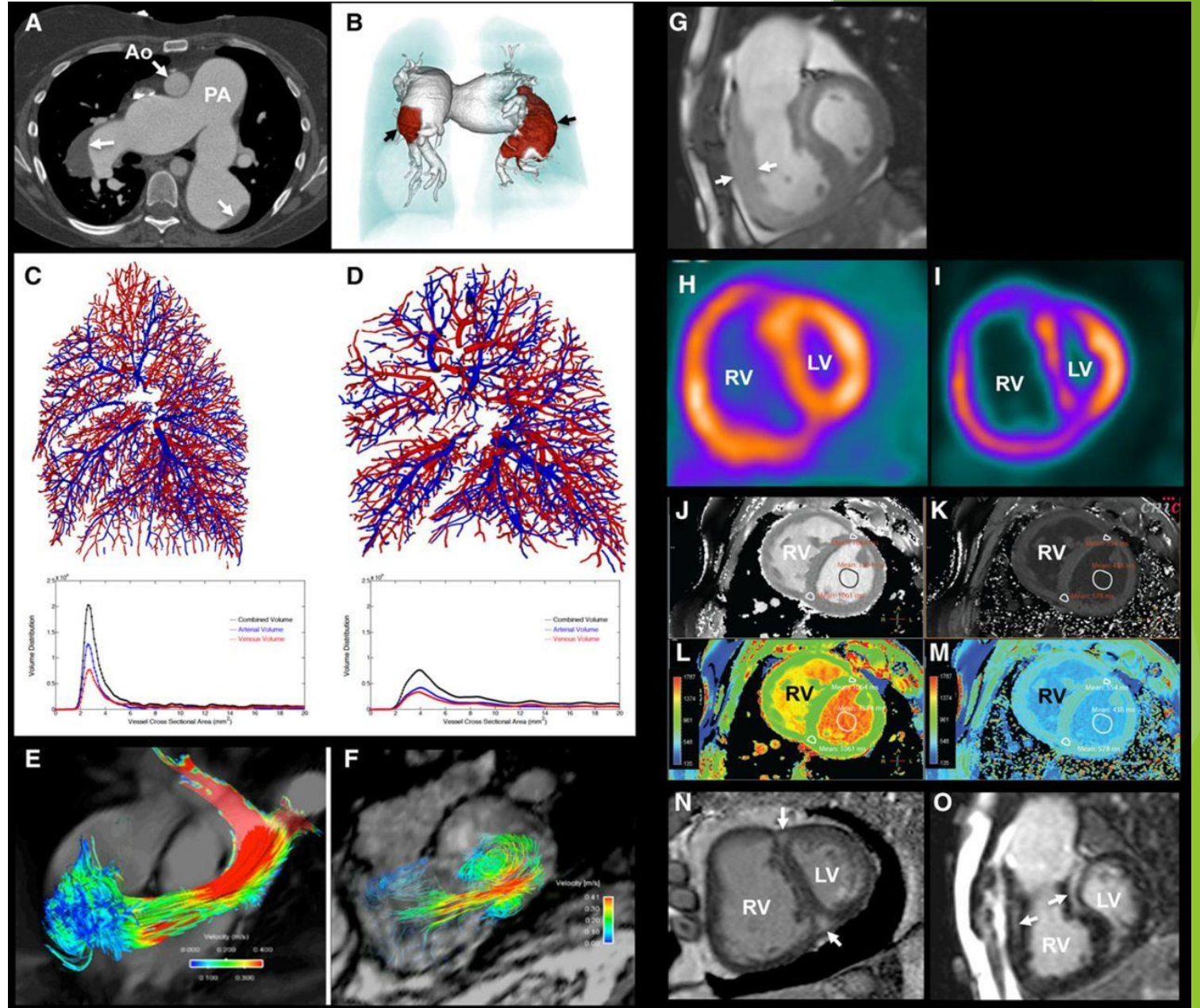


# Advancements in Cardiovascular Imaging

By Joe Doerer, MD

2/1/2025

Cardiac imaging frequently will complement each other to come up with a correct diagnosis and help facilitate a treatment plan.



# Introduction

- ▶ Echocardiogram
  - ▶ AI
  - ▶ 3D/4D
- ▶ Nuclear imaging
  - ▶ Cardiac amyloid
  - ▶ PET imaging
    - ▶ Aortic stenosis
    - ▶ Endocarditis
- ▶ Cardiac CT
  - ▶ Coronary artery disease
  - ▶ Photon-counting CT
  - ▶ CT perfusion
  - ▶ Structural planning
- ▶ Cardiac MRI
  - ▶ CardioOncology
  - ▶ Coronary artery disease
  - ▶ 4D Flow

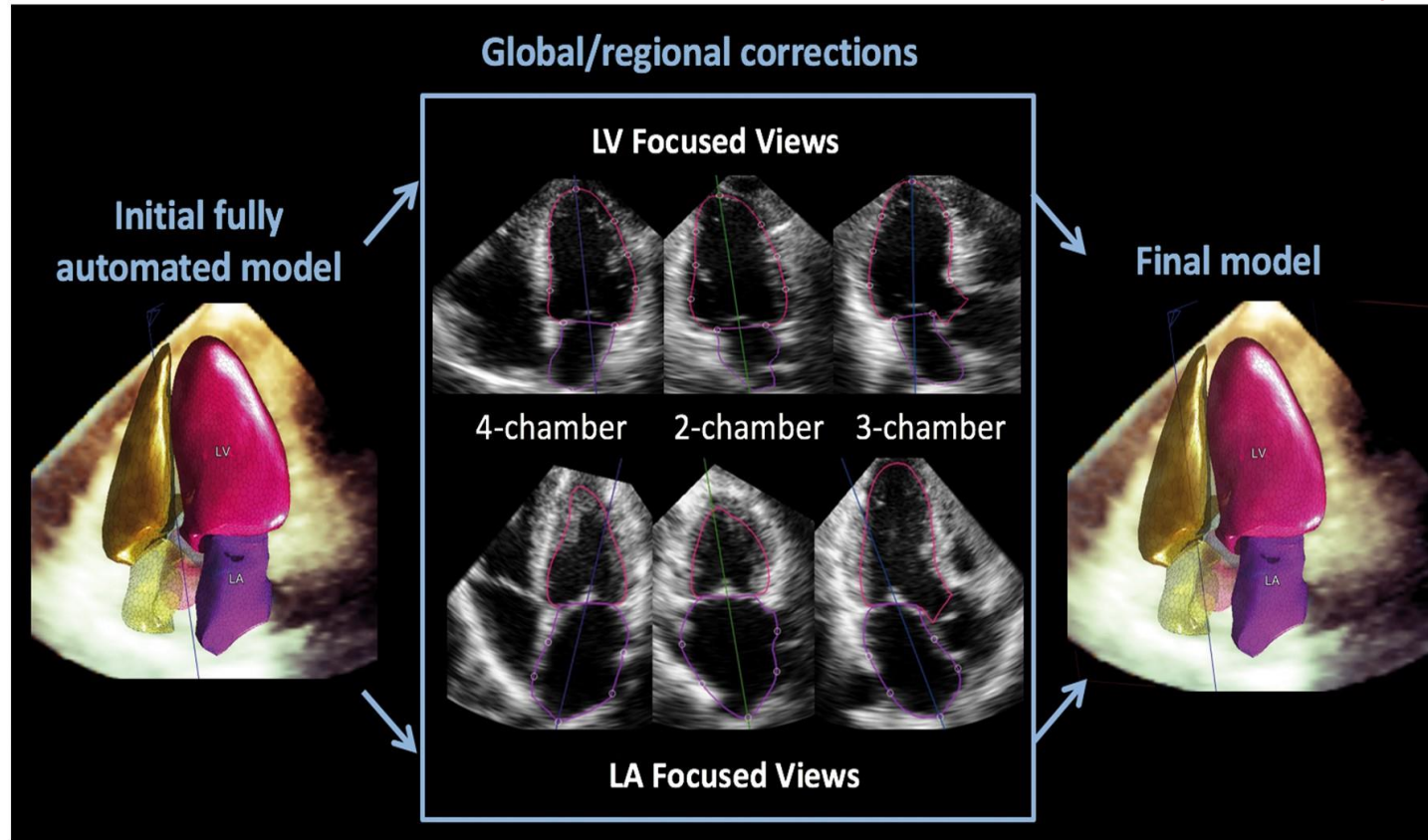


**Figure 2** Automated technique for left-heart 3D chamber quantification. Following initial fully-automated detection of left ventricular and left atrial endocardial surfaces (left), the software allows the user to perform manual corrections of the endocardial boundaries when needed (centre), resulting in final 3D casts of the cardiac chambers. The optional correction are performed in anatomically correct non-foreshortened 2D planes showing focused long-axis views of the left ventricle (top) and left atrium (bottom), both automatically extracted from the 3D dataset.

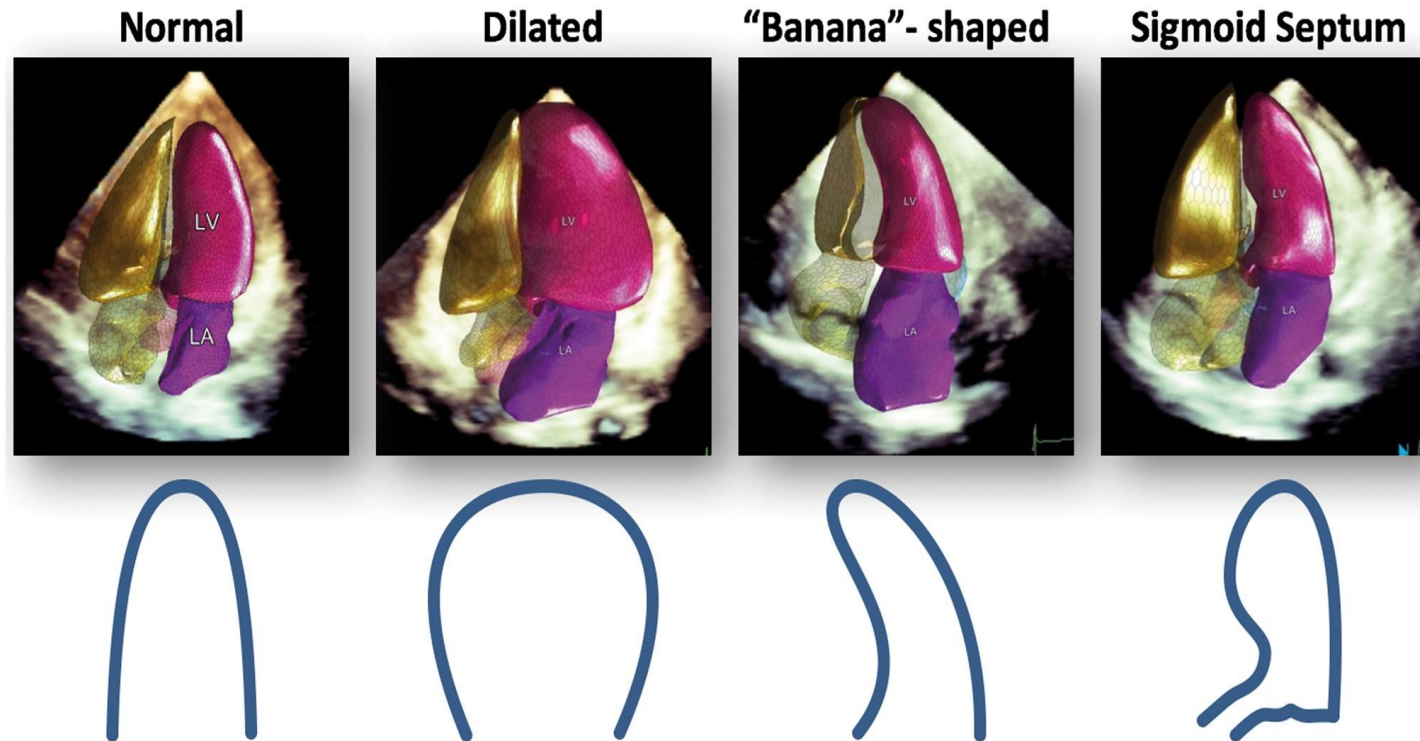


**Figure 1** Different left ventricular shapes that the automated software was trained to recognize. In addition to normal ventricles, the training set included a number of common abnormal/asymmetrical ventricular shapes. (Note that the program displays RV and RA casts but no volume values are provided because they have not been validated).

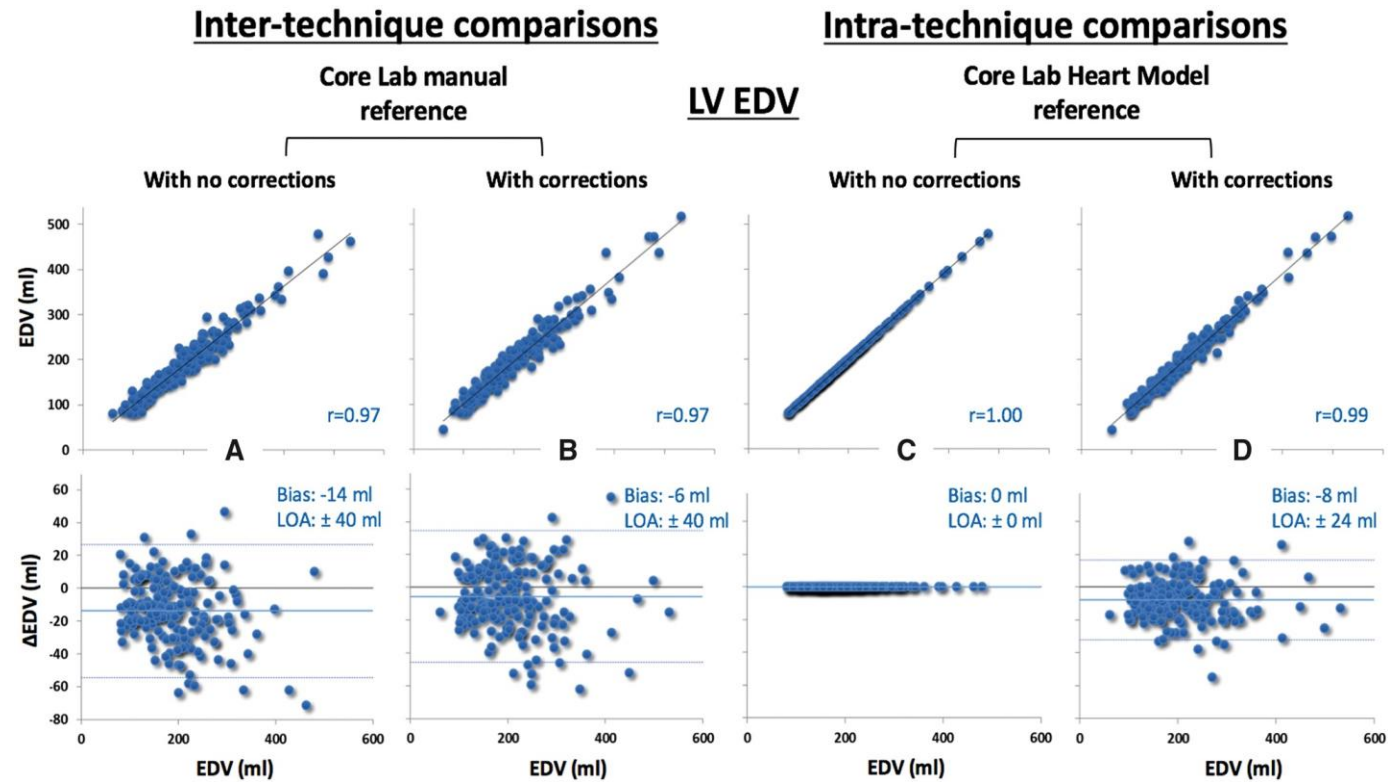


**Figure 3** Inter- and intra-technique comparisons for left ventricular end-diastolic volume. Correlation and Bland-Altman analysis for the automated measurements by the sites without and with contour correction against the conventional manual technique by the Core Lab (A and B, respectively), as well as against the corresponding automated technique by the Core Lab (C and D, respectively).

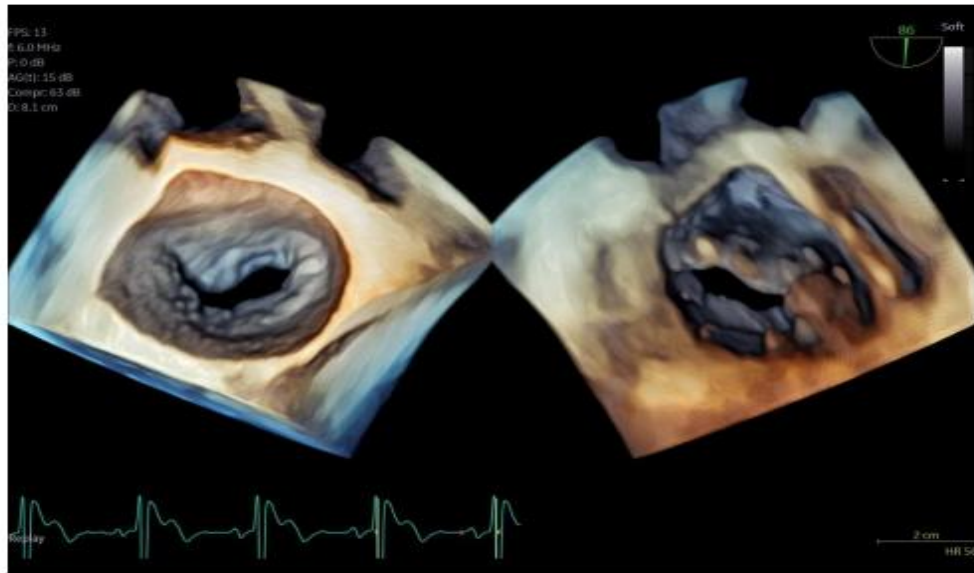


**Figure 3.** Dual crop 3D volume-rendered atrial (left) and ventricular (right) views of normal mitral valve.

- ▶ Papadopoulos K et al. Initial Experience with the 4D Mini-TEE Probe in the Adult Population. J. Clin. Med. 2024, 13, 6450.

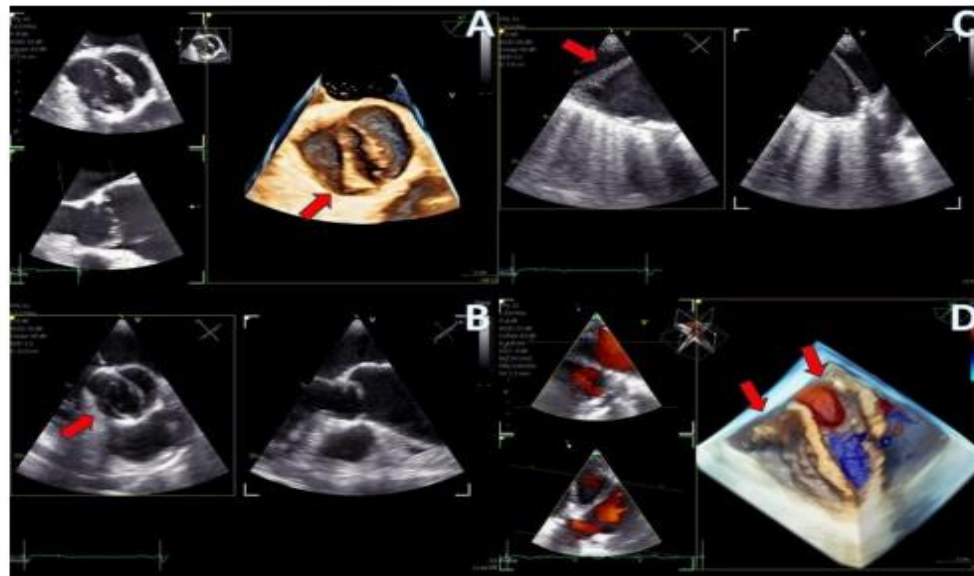


**Figure 4.** (A) A 4D demonstration of a true-bicuspid aortic valve (red arrow), (B) Biplane 2D demonstration of a true-bicuspid aortic valve (red arrow), (C) Chronic dissection of descending aorta (red arrow showing the wall of the true lumen), (D) 3D volume-rendered color Doppler image showing the true (right arrow) and the false lumen (left arrow).



Figure 5. Biplane images of tending of the atrial septum during trans-septal puncture for atrial fibrillation cryo-ablation.

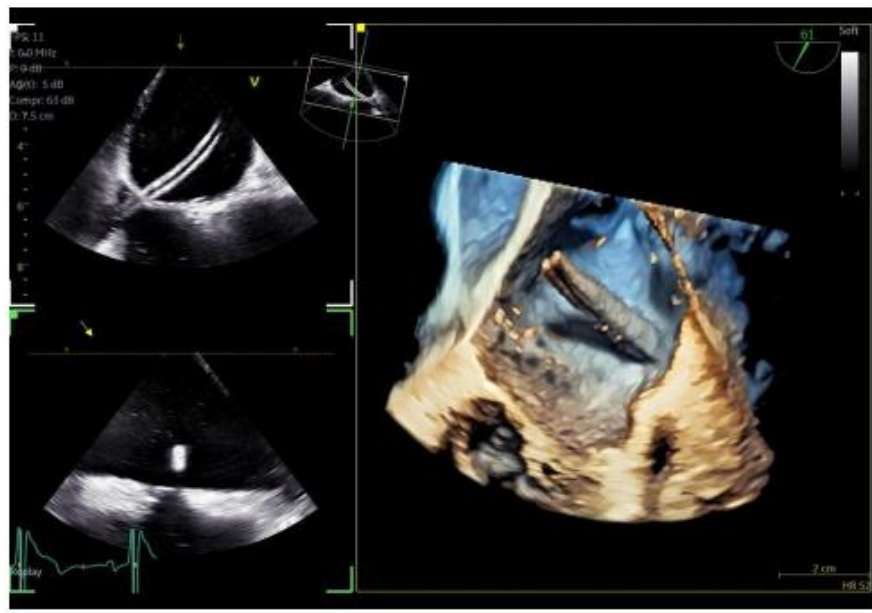


Figure 6. Azimuth level (top left), elevation level (bottom left), and 3D volume-rendered image (right) of an SL0 catheter for the guidance of cryo-ablation procedure.

Papadopoulos K et al.  
Initial Experience with the  
4D Mini-TEE Probe in the  
Adult Population. J. Clin.  
Med. 2024, 13, 6450.

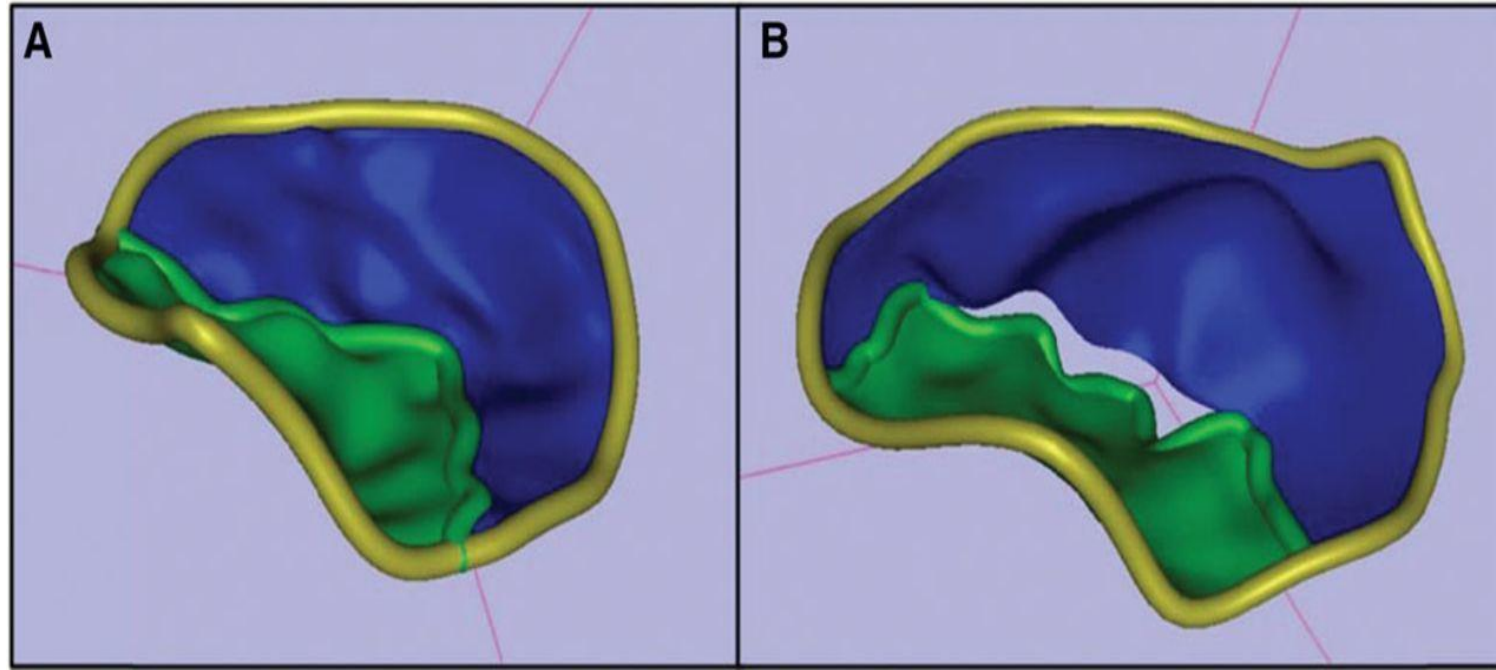


Figure 1. Two patient-specific static mitral valve models: normal patient (A) and organic mitral regurgitation patient (B), both at midsystole. Color scheme: Mitral annulus in gold, anterior leaflet in green, and posterior leaflet in blue.



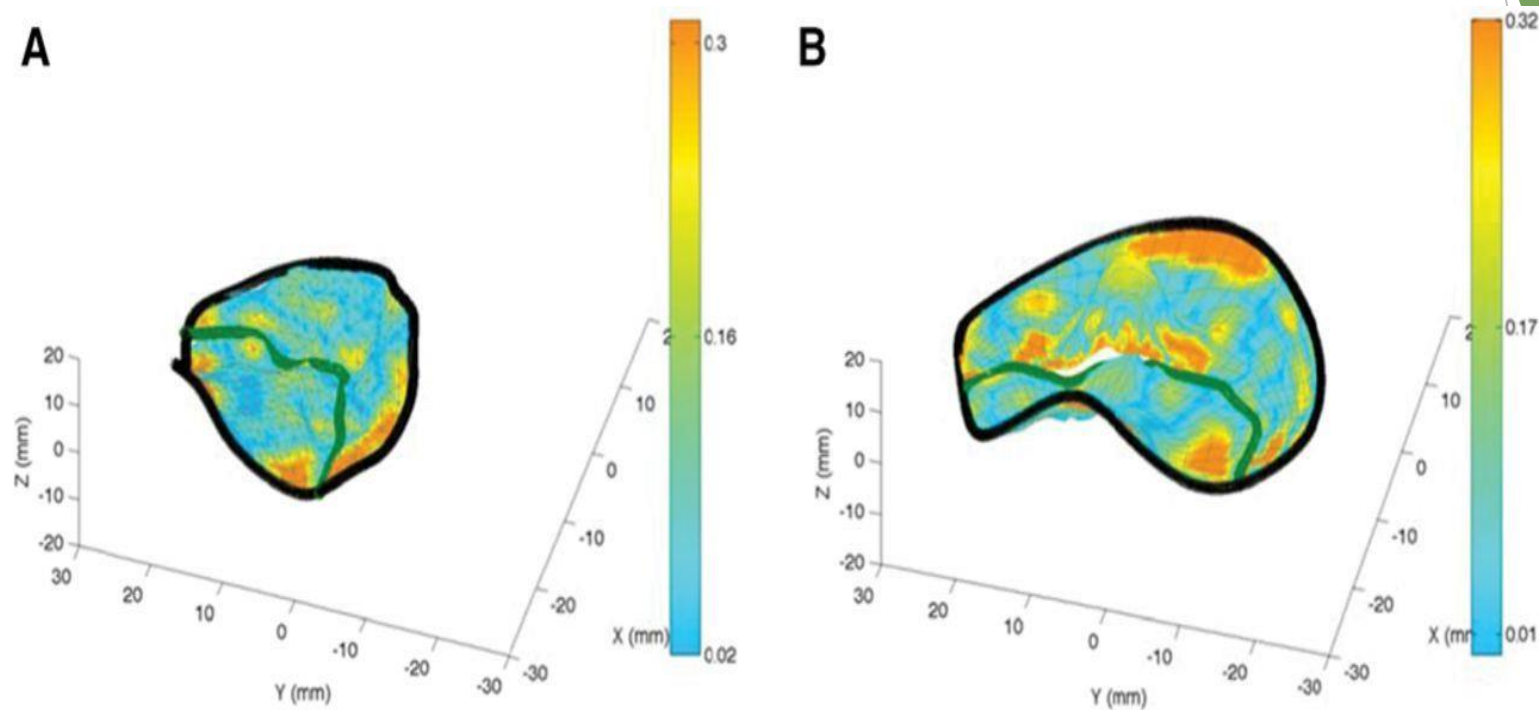
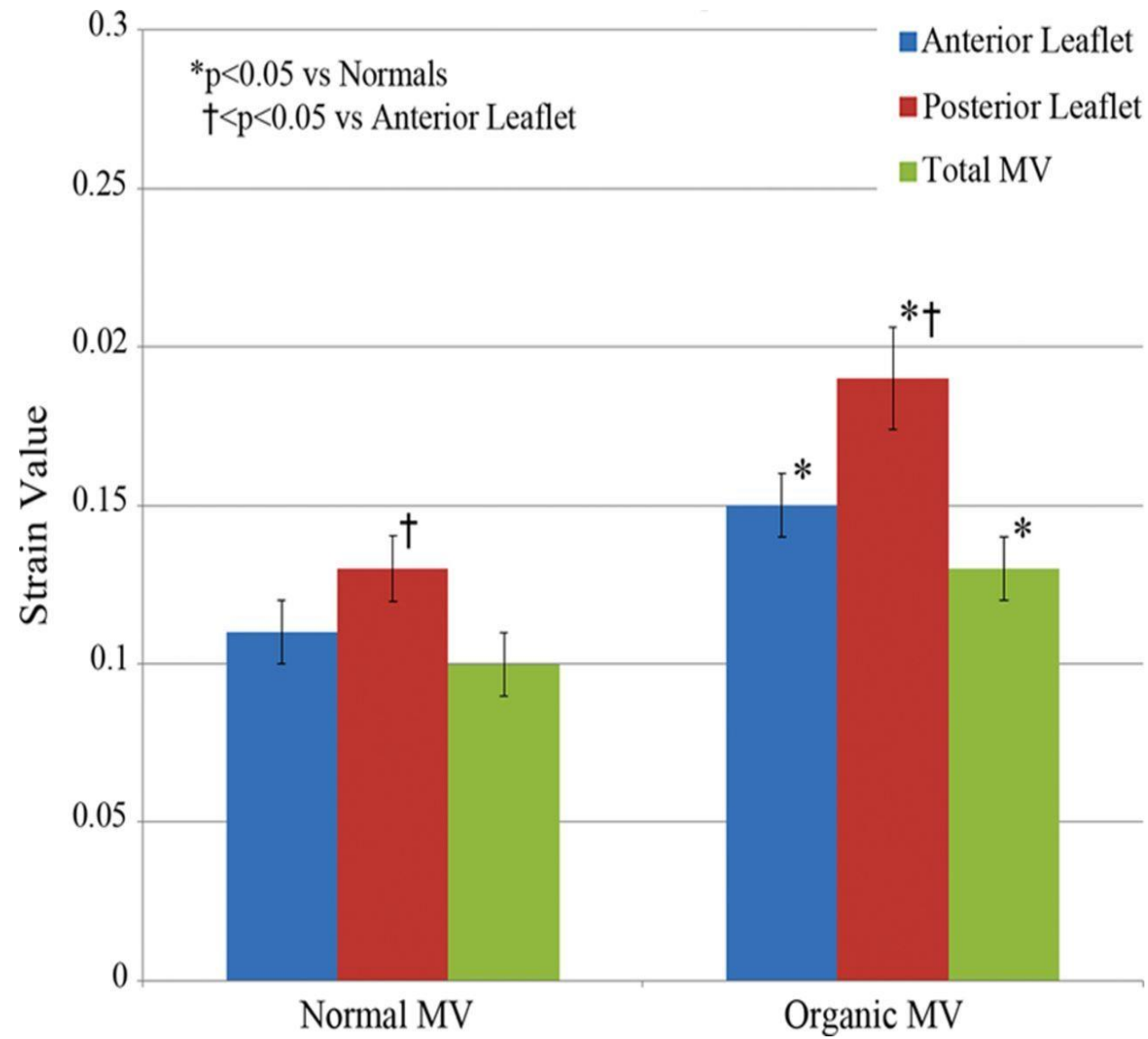


Figure 3. Patient-specific mitral leaflets strain intensities displayed at midsystole for a typical normal mitral valve (A) and for a typical organic valve with mitral regurgitation valve (B). The strain intensities color code range from dark orange for high strain to dark blue for low strain.





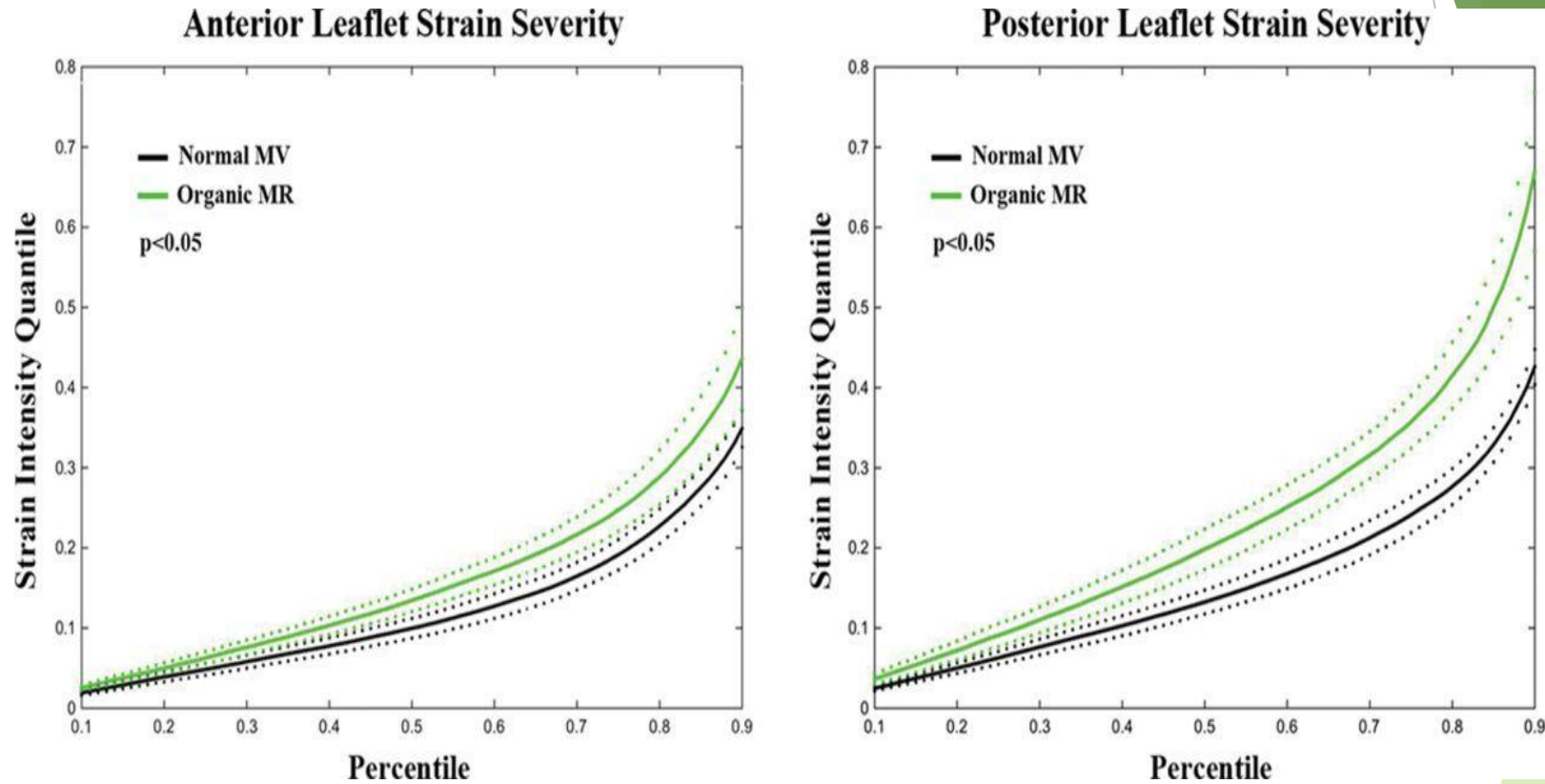


Figure 6. Mean strain percentile curves and respective 95% confidence limits in anterior and posterior leaflets of normal mitral valves (MVs) and organic mitral regurgitation. Strain values are higher in organic mitral regurgitation (MR) than in normal valves. 18



From: **Cardiac Amyloidosis Due to Transthyretin Protein: A Review**

JAMA. 2024;331(9):778-791. doi:10.1001/jama.2024.0442

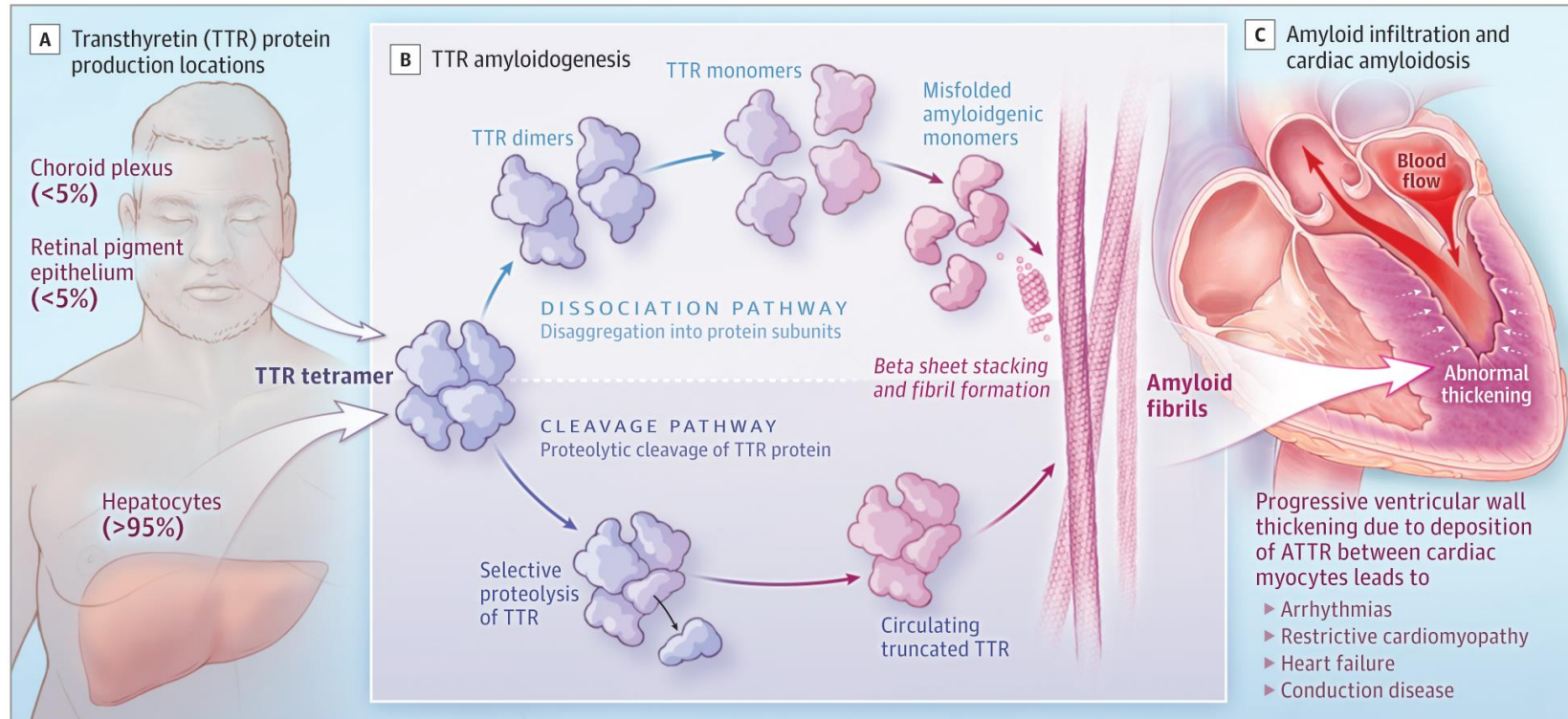


Figure Legend:

Pathobiology of ATTR Amyloidosis and Cardiac Manifestations Circulating TTR protein is synthesized by the liver as a homotetramer that dissociates or is proteolytically cleaved into intermediates that misfold and ultimately organize into amyloid fibrils. Amyloid fibrils then deposit in the heart, resulting in arrhythmia, conduction disease often requiring placement, and heart failure.

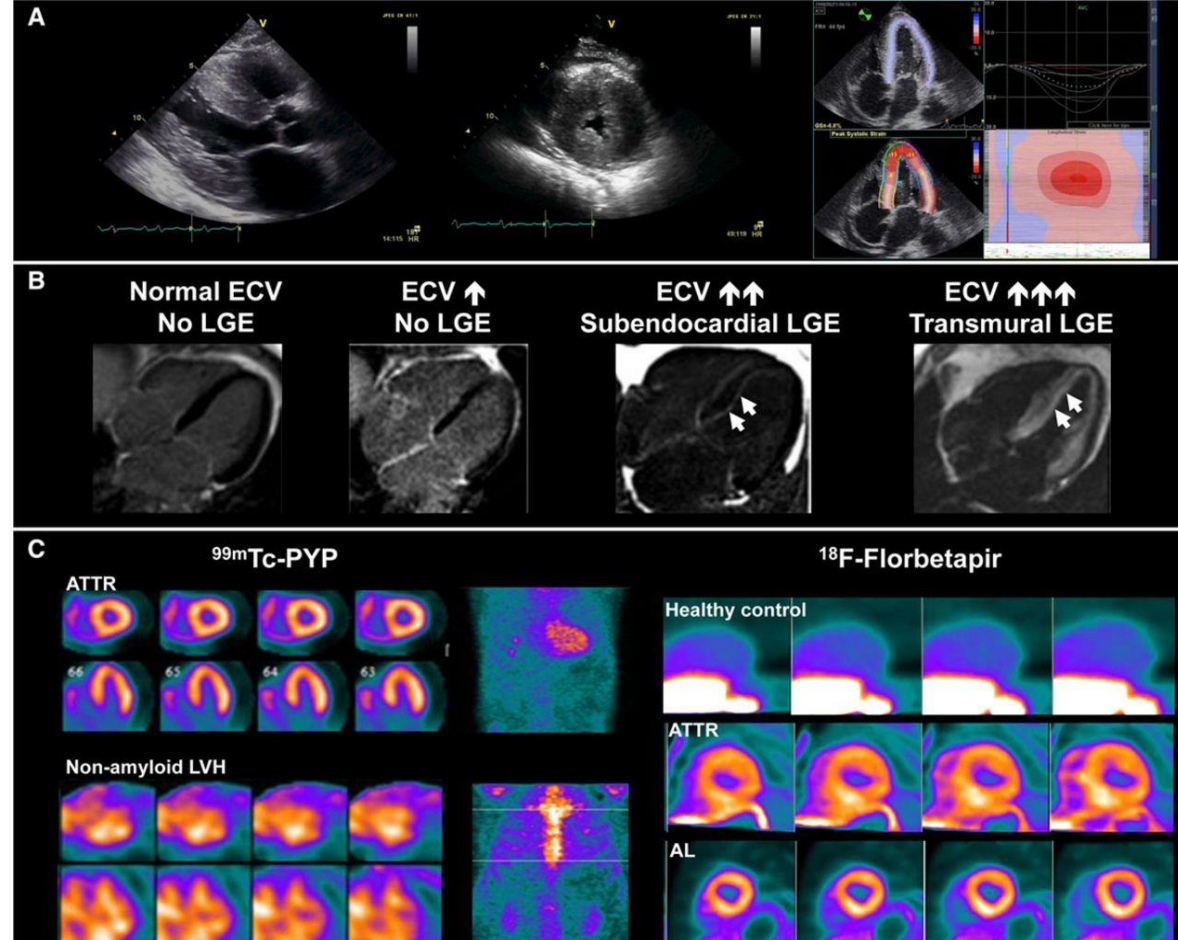


Figure 6. Multimodality imaging of cardiac amyloidosis. **A**, 2D echocardiographic images demonstrating severe concentric LVH (Left and Center) and reduced circumferential strain involving only the base of the LV (images courtesy of Dr Frederick Ruberg). **B**, Representative transaxial MRI images representing the assumed progression of amyloid deposition in the heart over time. The earliest stages of amyloid infiltration demonstrate an expansion of the extracellular volume (ECV), quantified by T1 mapping, without obvious late gadolinium enhancement (LGE). With continued amyloid deposition, there is an increase in ECV and the appearance of subendocardial LGE (arrows). In the advanced stages of the disease, there is further increase in ECV and a progression to transmural LGE. Images are modified from Fontana et al<sup>71</sup> with permission of the publisher. **C**, Molecular imaging of cardiac amyloid deposits using <sup>99m</sup>Tc-pyrophosphate (PYP) SPECT, and <sup>18</sup>F-florbetapir PET imaging. The PYP images demonstrate intense myocardial uptake primarily in transthyretin (TTR) amyloidosis, but not in nonamyloid LVH. Light chain cardiac amyloidosis (AL) generally shows no or very mild tracer uptake on bone scintigraphy. <sup>18</sup>F-Florbetapir uptake is typically present in both forms of amyloidosis, but quantitatively higher in AL than TTR. No uptake is seen in nonamyloid LVH. LVH indicates left ventricular hypertrophy; and SPECT, single-photon emission computed tomography.



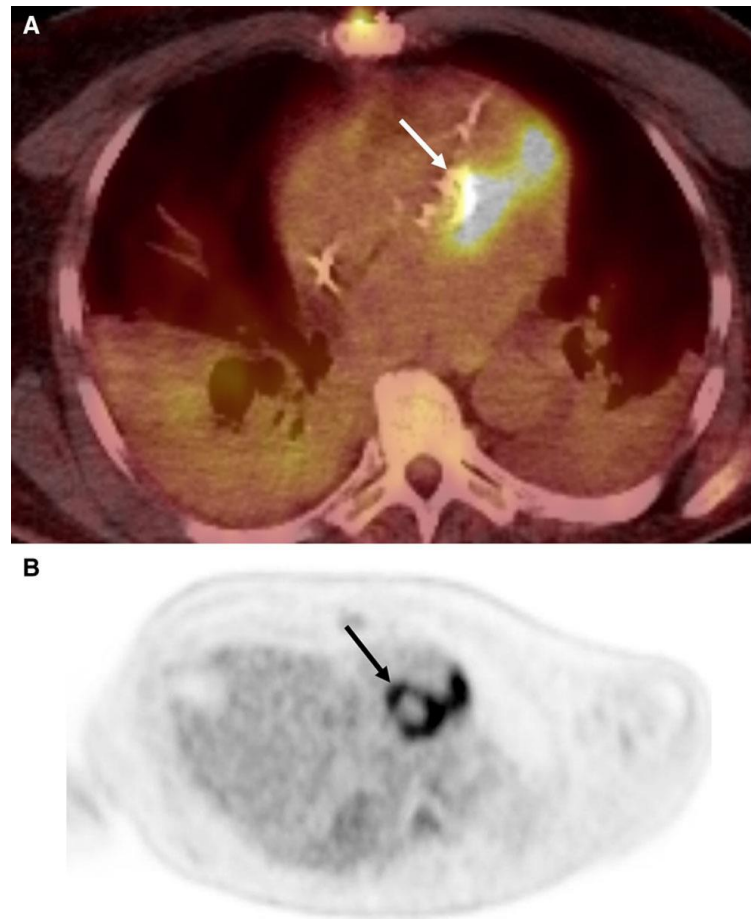


Figure 6. 18F-fluorodeoxyglucose positron emission tomography (PET)/computed tomography scan demonstrating aortic root abscess (arrow) and tracking of infection along basal anterior interventricular septum on (A) standard PET and (B) time of flight imaging.



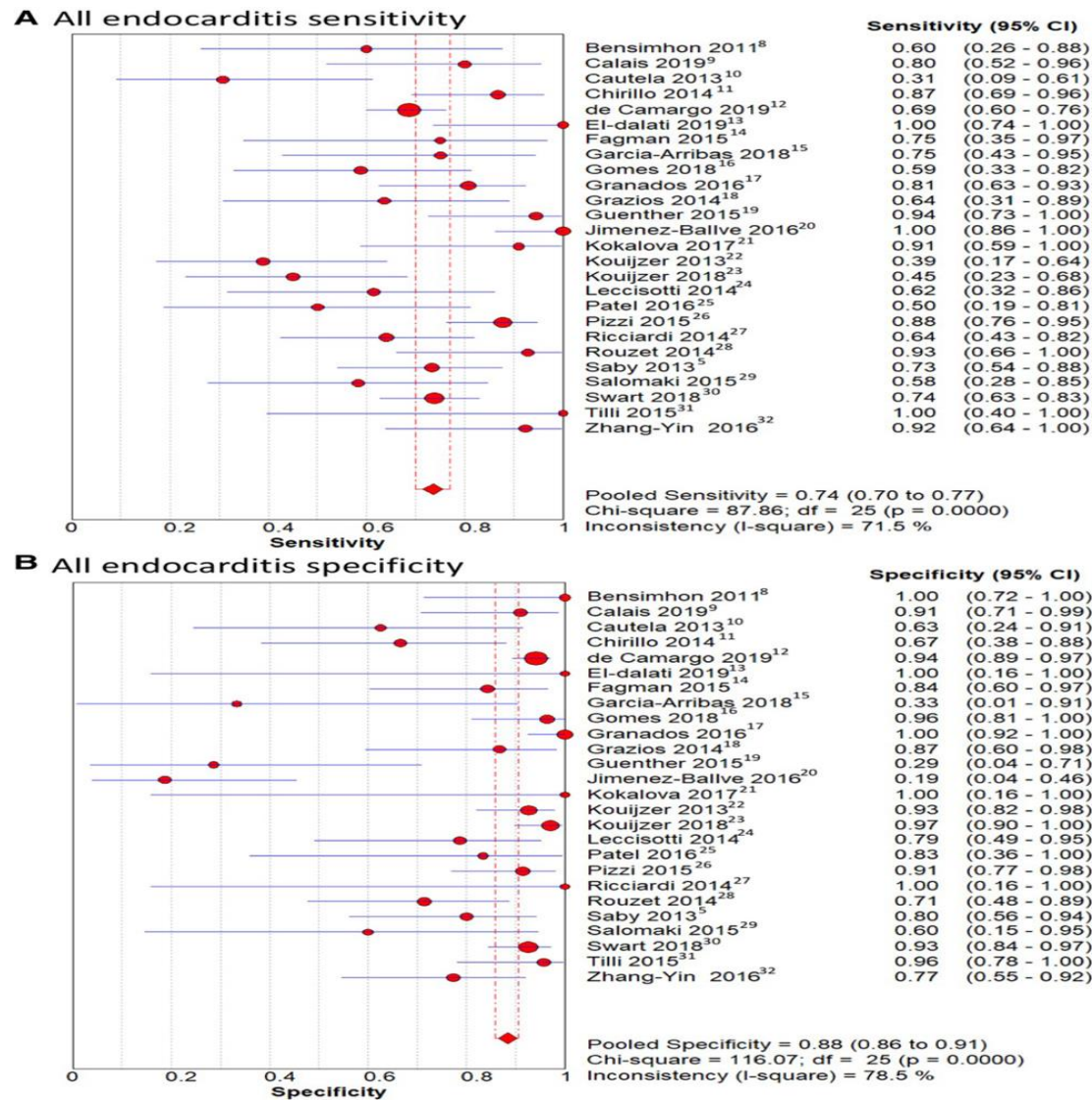


Figure 2. Forrest plots of pooled data for 18F-fluorodeoxyglucose positron emission tomography/computed tomography to detect all infective endocarditis. A, pooled sensitivity and; B, pooled specificity.



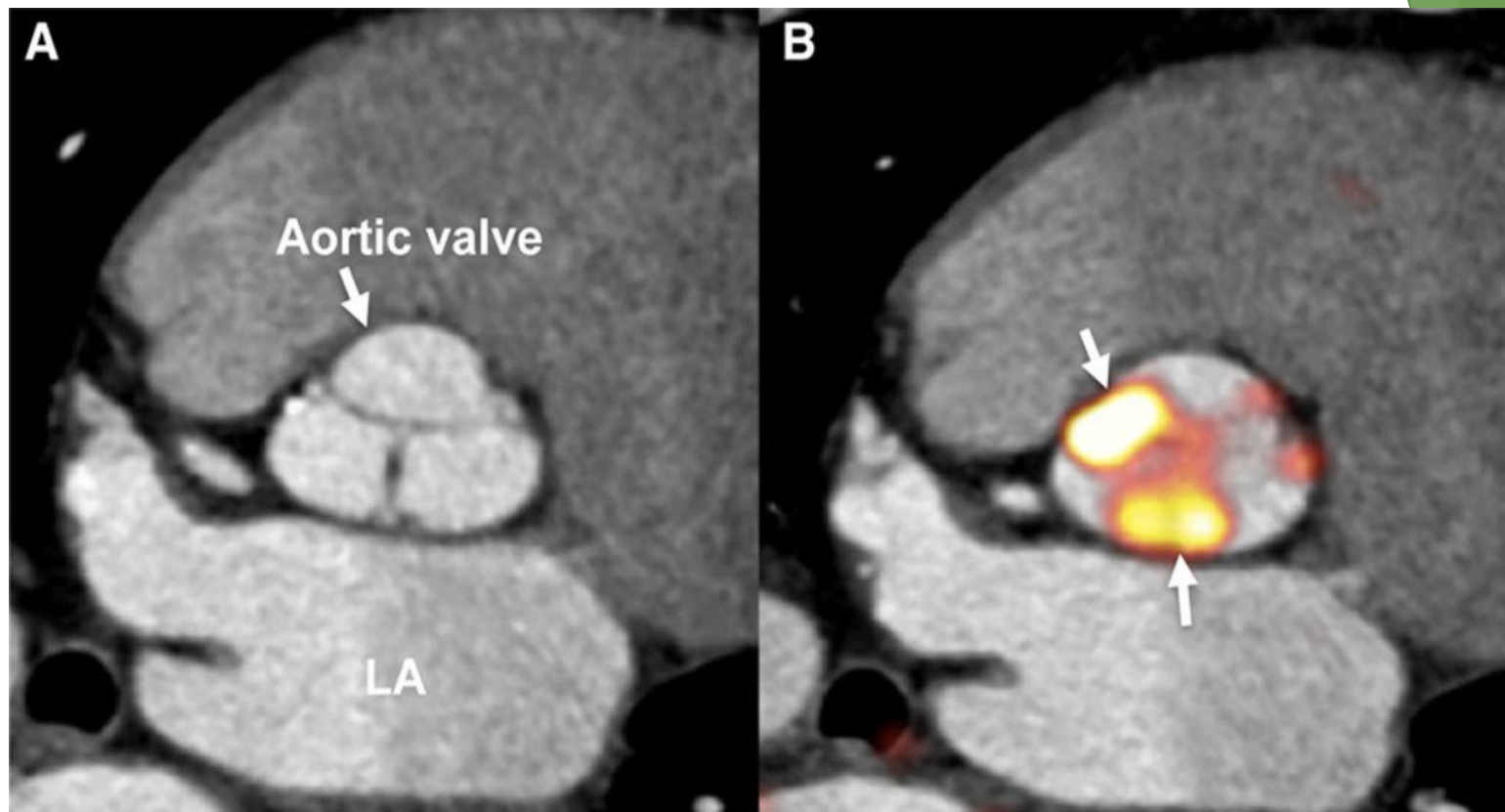


Figure 2. Targeted PET-CT imaging of aortic valve disease. A, Contrast-enhanced computed tomographic (CT) multiplanar reformatted views of the aortic valve and aortic root, with fused targeted images of calcium metabolism obtained with sodium fluoride (NaF) positron emission tomography (PET). B, Increased NaF uptake (arrows), reflecting active calcium deposition, despite no evidence of macroscopic calcifications on CT (images courtesy of Dr Marc Dweck, University of Edinburgh, England). LA indicates left atrium.



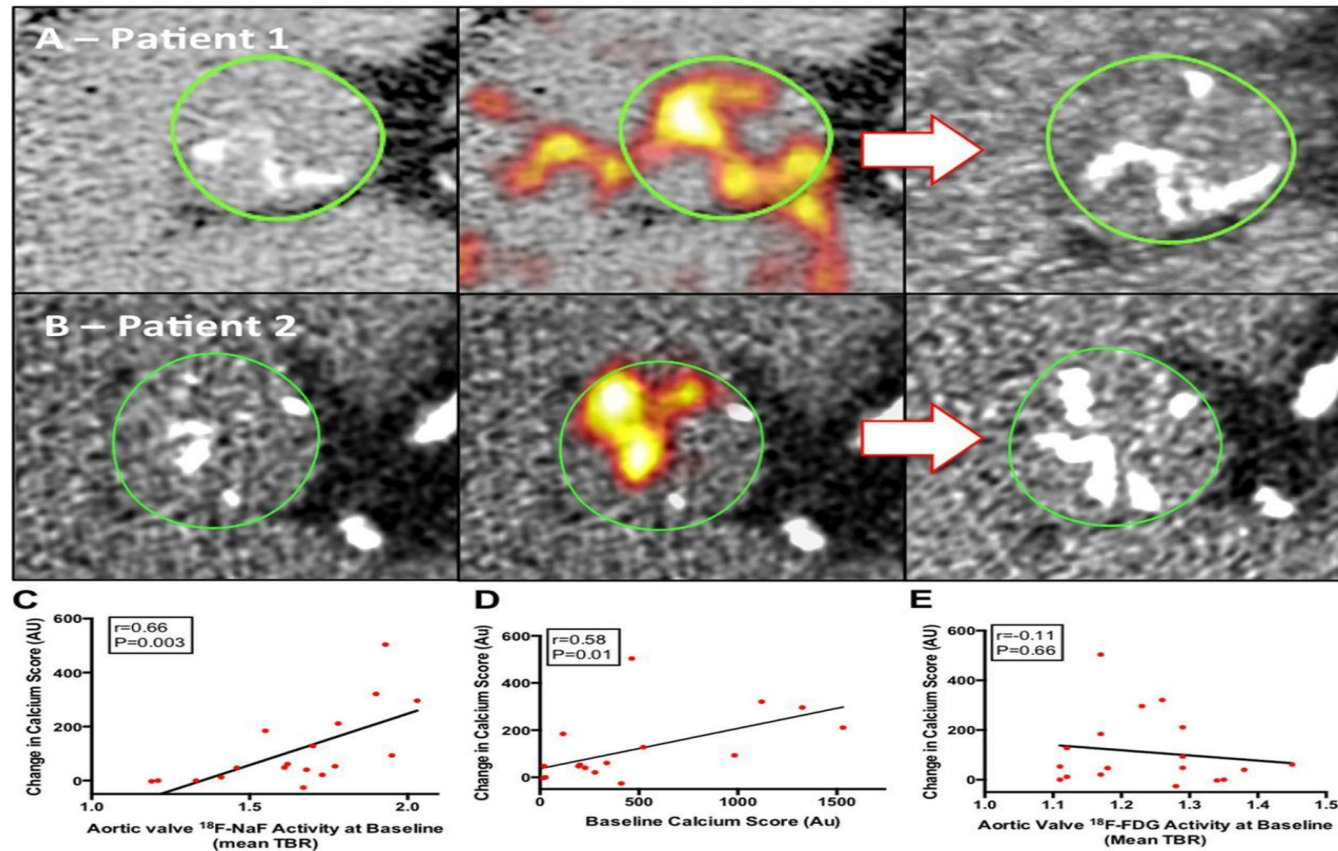


Figure 3. Change in aortic valve computed tomography (CT) calcium score and  $^{18}\text{F}$ -sodium fluoride (NaF) positron emission tomography (PET) activity after 1 year. A and B, Coaxial short axis views of the aortic valve from 2 patients with mild aortic stenosis (top and bottom). On baseline CT scans (left) established regions of macrocalcification appear white. Baseline fused  $^{18}\text{F-NaF}$  PET and CT scans (middle) show intense  $^{18}\text{F-NaF}$  uptake (red, yellow regions) both overlying and adjacent to existing calcium deposits on the CT. One-year follow-up CT scans (right) demonstrate increased calcium accumulation in much the same distribution as the baseline PET activity. C-E, Predictors of progression in aortic valve calcium score. An excellent correlation was observed between baseline  $^{18}\text{F-NaF}$  activity in the aortic valve and the subsequent change in calcium score at 1 year  $r=0.66$ ,  $P<0.01$  (A). This matched the current gold standard predictor of disease progression the baseline calcium score  $r=0.58$ ,  $P=0.01$  (B). By contrast, there was a poor correlation with  $^{18}\text{F}$ -fluorodeoxyglucose (FDG) activity in the valve  $r=-0.11$ ,  $P=0.66$  (C).



## Pretest Probabilities of Obstructive CAD in Symptomatic Patients

(A) according to age, sex, and symptoms;

(B) according to age, sex, symptoms, and CAC

Age, y	Chest Pain		Dyspnea	
	Men	Women	Men	Women
30–39	≤4	≤5	0	3
40–49	≤22	≤10	12	3
50–59	≤32	≤13	20	9
60–69	≤44	≤16	27	14
70+	≤52	≤27	32	12

**A** Pretest probability based on age, sex, and symptoms



**B** Pretest probability based on age, sex, symptoms, and CAC score<sup>+</sup>

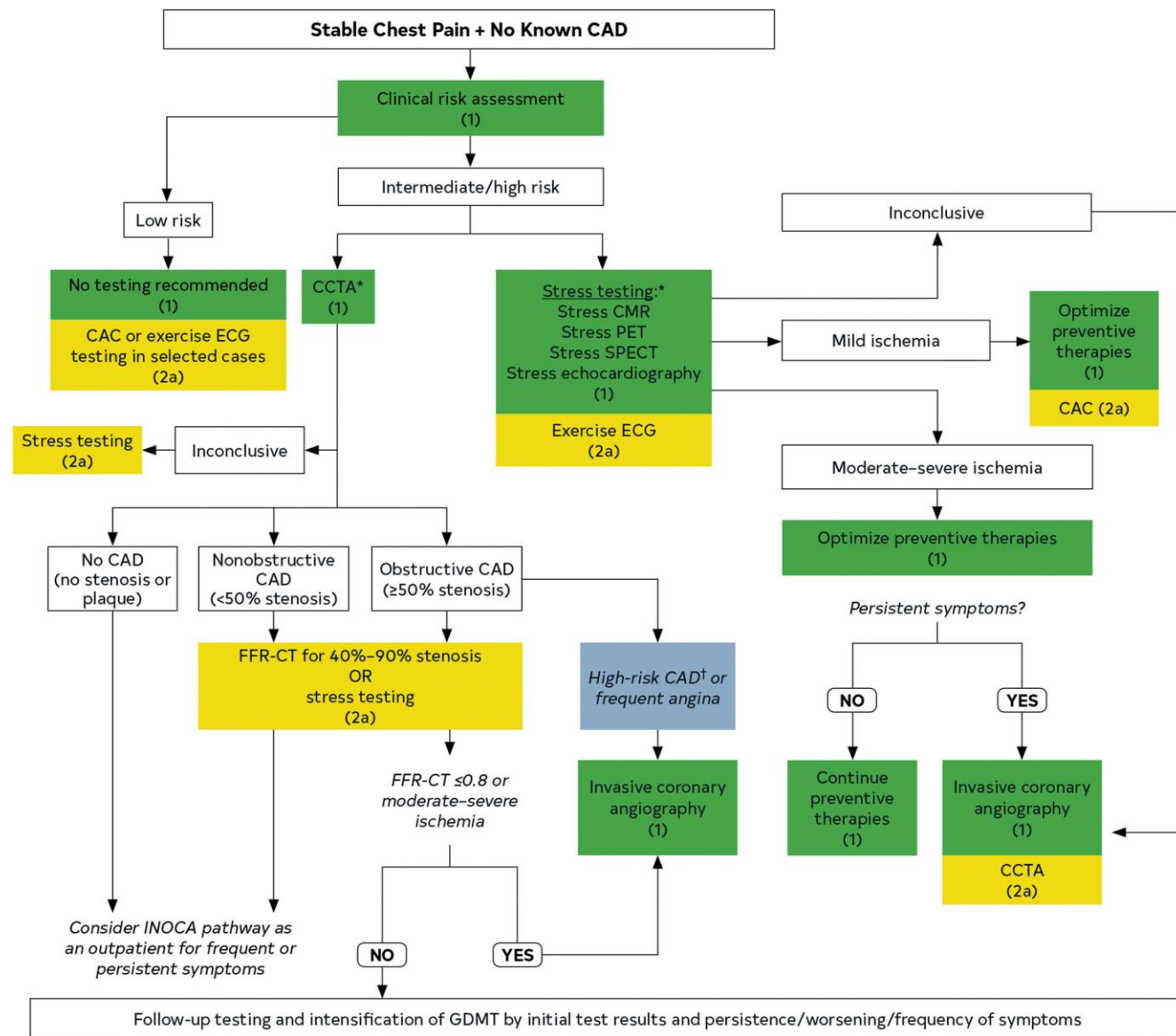


CAC  
1–99

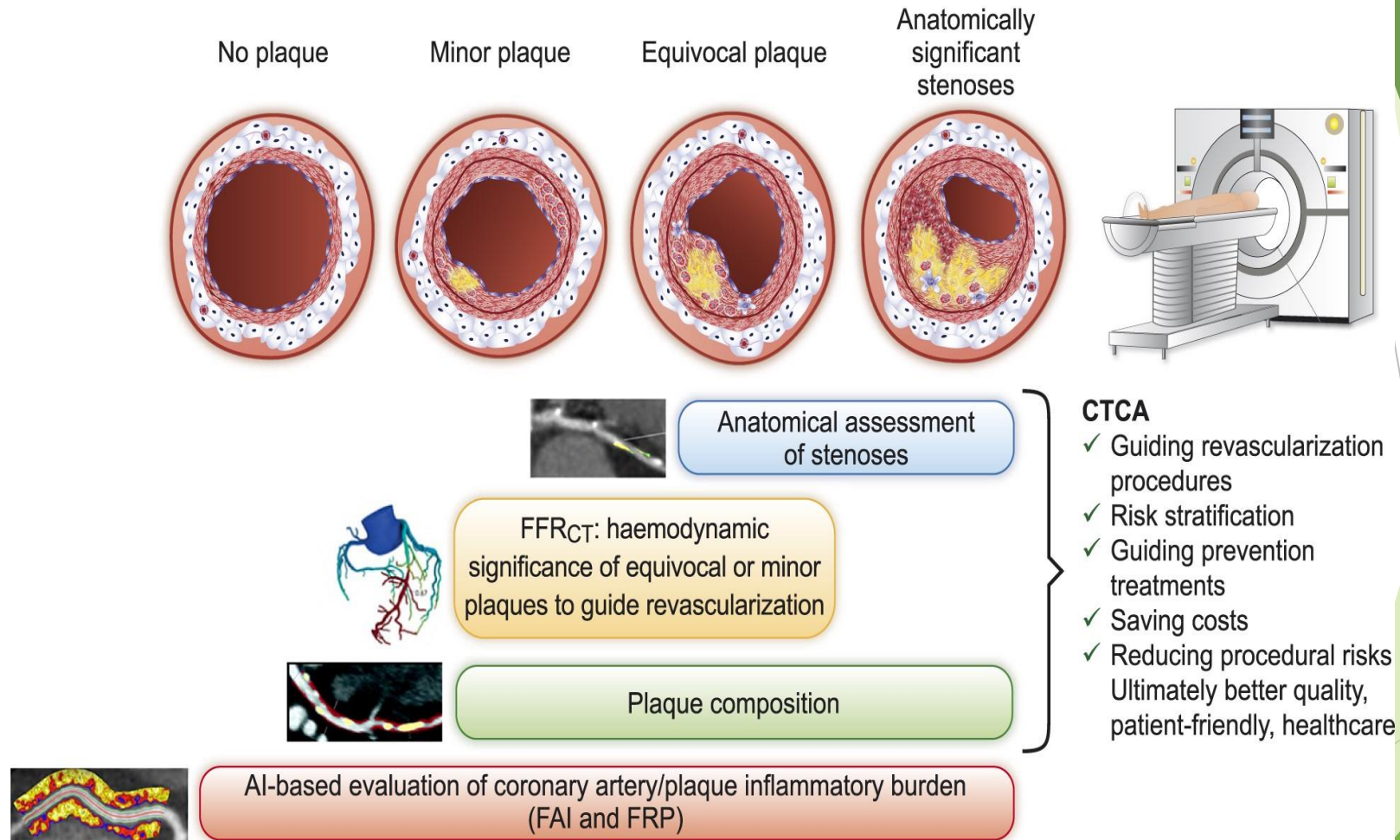
CAC  
≥100–999

CAC  
≥1,000





**CTCA as one-stop-shop for chest pain investigation:  
Positioning FFR<sub>CT</sub> in clinical care and maximizing the yield of the test prediction and prevention management.**



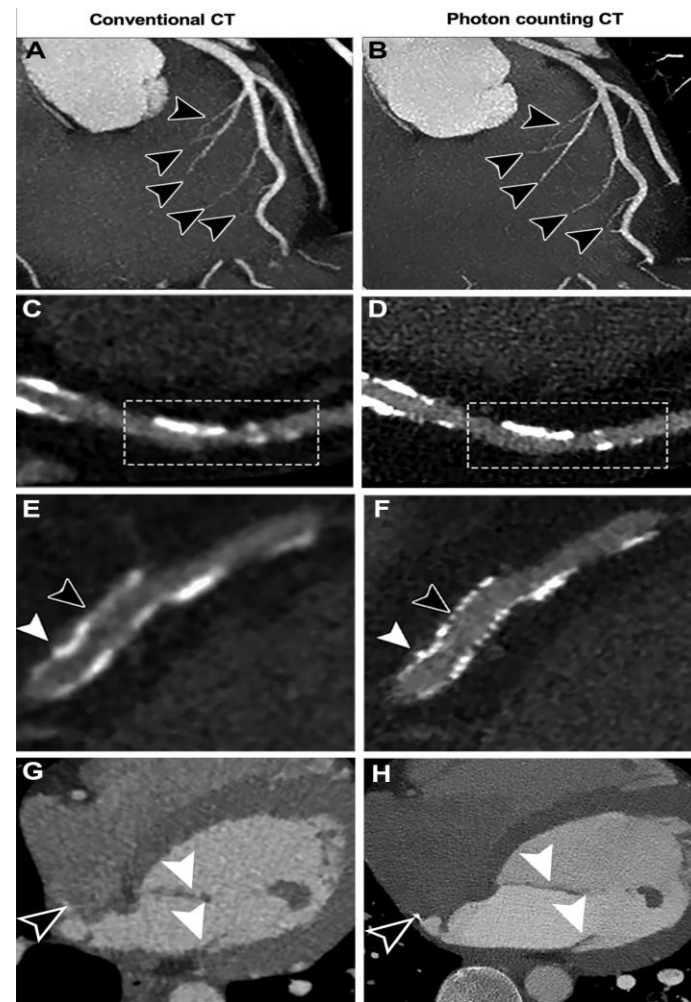


Figure 10: Images from conventional CT (left) and photon-counting CT (right) for cardiac evaluation. **(A, B)** CT scans show that septal branches (arrowheads) are better depicted on maximum-intensity projections with photon-counting CT **(B)** than with conventional CT **(A)**. **(C, D)** Curved planar reconstructions show that calcifications (inside the box) are more differentiable from the lumen on photon-counting CT scans **(D)** compared with conventional CT scans **(C)**. **(E, F)** CT scans show that a stent (black arrowhead) and an outside calcification (white arrowhead) with focal disruption of the struts are better depicted with photon-counting CT **(F)** than with conventional CT **(E)**. **(G, H)** CT scans show that mitral leaflets (white arrowheads) and calcification in a left atrial diverticulum (black arrowhead) are better depicted with photon-counting CT **(H)** than with conventional CT **(G)**. (Adapted, with permission, from reference 68.)



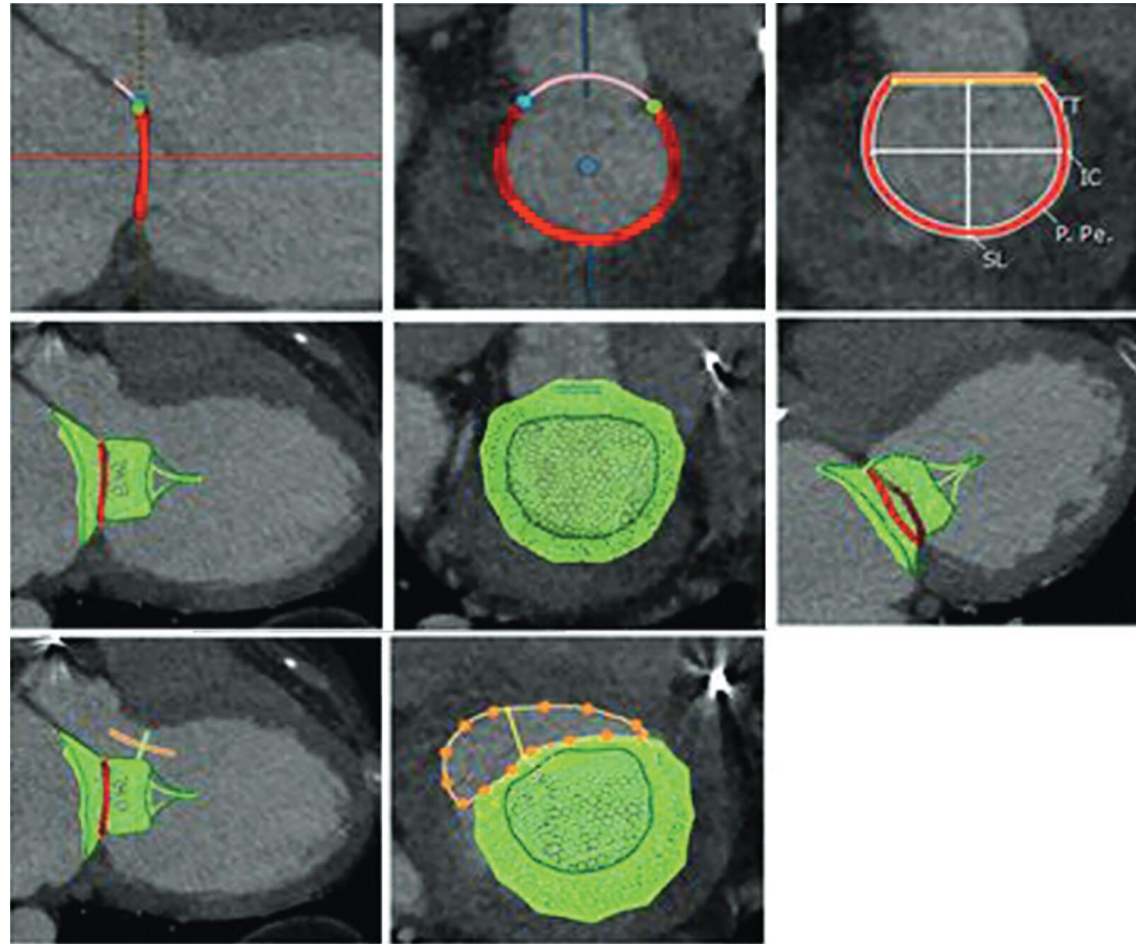
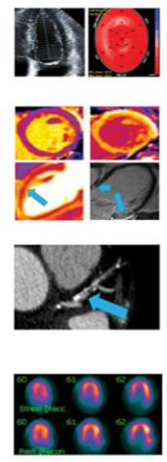


Figure 6: Cardiac CT images for planning transcatheter mitral valve replacement. Top: Images show the multipoint segmentation arc (red line) of the d-shaped mitral valve annulus. Annulus size (area, septolateral [SL], and intercommissural [IC] distance) is used to determine eligibility for, and sizing of, the transcatheter mitral valve replacement. Middle: Images show a simulated virtual transcatheter mitral valve replacement (in this example, a Tendyne [Abbott Vascular] device is indicated in green), which can be manually adjusted for size and placed across the mitral annulus (red line). Bottom: Images show the center line technique drawn along the trajectory of the left ventricular outflow tract (LVOT; orange line). A cross-sectional area (curved dotted orange line) across the narrowest point of the LVOT forms the neo-LVOT (6.5 cm<sup>2</sup> in this case). (Reprinted, under a CC BY license, from reference 33.)

**A Use of Cardiac Imaging Along the Spectrum of Cancer Treatment**

Before Treatment	During Treatment	After Treatment
<b>Echocardiography</b>		
LV Function Assessment Cardiac mass Valvular disease	LV Function Assessment Consider as needed for cardiac mass, or Other significant cardiovascular states (eg, valve disease)	LV Function Assessment Consider as needed for cardiac mass, or Other significant cardiovascular states (eg, valve disease)
<b>Cardiac Magnetic Resonance (CMR)</b>		
Unexplained heart failure Recent myopericarditis Accurate LVEF or valve assessment before cancer treatment Cardiac mass assessment Cardiac amyloid	Unexplained heart failure Recent myopericarditis Accurate LVEF or valve assessment before cancer treatment Cardiac mass assessment Consider as needed other cardiovascular states (eg, amyloid)	Unexplained heart failure Recent myopericarditis Accurate LVEF or valve assessment before cancer treatment Cardiac mass assessment Consider as needed other cardiovascular states (eg, amyloid)
<b>Cardiac Computed Tomography (CCT)</b>		
Symptomatic CAD evaluation prior to pro-ischemic or prothrombotic treatment Guidance of primary prevention therapy with intermediate ASCVD risk Structural planning before TAVR or TMVR	Use as needed for general symptoms (eg, suspected CAD)	Use as needed for general symptoms (eg, suspected CAD)
<b>Nuclear or Positron Emission Tomography (PET)</b>		
Symptomatic CAD evaluation prior to pro-ischemic or prothrombotic treatment Cardiac Amyloid Metabolic activity of cardiac mass	Use as needed for general symptoms (eg, suspected CAD) Consider as needed for cardiac mass, or other cardiovascular states (eg, amyloid)	Use as needed for general symptoms (eg, suspected CAD) Consider as needed for cardiac mass, or other cardiovascular states (eg, amyloid)

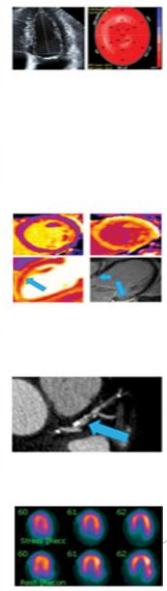
**Modality**



**B Suggested Cardiac Imaging Strategy, by Cancer Treatment type**

Before Treatment	During Treatment	After Treatment
<b>Echocardiography (Echo)</b>		
Initiation of any of the following*: • Anthracyclines • HER2 Targeted • Immune Checkpoint Inhibitor • CAR-T cell • VEGF Inhibitor • BTK Inhibitor • Proteasome Inhibitor • Radiation • Stem Cell Transplant • Fluoropyrimidines (eg, FU-5) Cardiac Amyloid*	Consider at least 1 assessment: • Anthracyclines • HER2 Targeted • Proteasome Inhibitor and Symptoms with any of the following: • Immune Checkpoint Inhibitor • CAR-T cell • VEGF Inhibitor • BTK Inhibitor • Radiation • Stem Cell Transplant • Fluoropyrimidines (eg, FU-5)	Consider at least 1 assessment: • Anthracyclines • HER2 Targeted • Proteasome Inhibitor and Symptoms with any of the following: • Immune Checkpoint Inhibitor • CAR-T cell • VEGF Inhibitor • BTK Inhibitor • Radiation • Stem Cell Transplant • Fluoropyrimidines (eg, FU-5)
<b>Cardiac Magnetic Resonance (CMR)</b>		
Consider if otherwise indicated Cardiac Amyloid*	Consider where needed if symptoms with any of the following: • Anthracyclines • HER2 Targeted • Immune Checkpoint Inhibitor • CAR-T cell • VEGF Inhibitor • BTK Inhibitor • Radiation • Stem Cell Transplant • Fluoropyrimidines (eg, FU-5)	Consider where needed if symptoms with any of the following: • Anthracyclines • HER2 Targeted • Immune Checkpoint Inhibitor • CAR-T cell • VEGF Inhibitor • BTK Inhibitor • Radiation • Stem Cell Transplant • Fluoropyrimidines (eg, FU-5)
<b>Cardiac Computed Tomography (CCT)</b>		
Consider if otherwise indicated Cardiac Amyloid*	Consider where needed if symptoms with any of the following: • Immune Checkpoint Inhibitor • Proteasome Inhibitor • Radiation • Stem Cell Transplant • Fluoropyrimidines (eg, FU-5)	Consider where needed if symptoms with any of the following: • Immune Checkpoint Inhibitor • Proteasome Inhibitor • Radiation • Stem Cell Transplant • Fluoropyrimidines (eg, FU-5) • CHIP mutations
<b>Nuclear (or PET) Imaging</b>		
Consider if otherwise indicated Cardiac Amyloid*	Consider where needed if symptoms with any of the following: • Immune Checkpoint Inhibitor • Proteasome Inhibitor • Radiation • Stem Cell Transplant • Fluoropyrimidines (eg, FU-5) Consider as needed for cardiac amyloid	Consider where needed if symptoms with any of the following: • Immune Checkpoint Inhibitor • Proteasome Inhibitor • Radiation • Stem Cell Transplant • Fluoropyrimidines (eg, FU-5) • CHIP mutations Consider as needed for cardiac amyloid

**Modality**



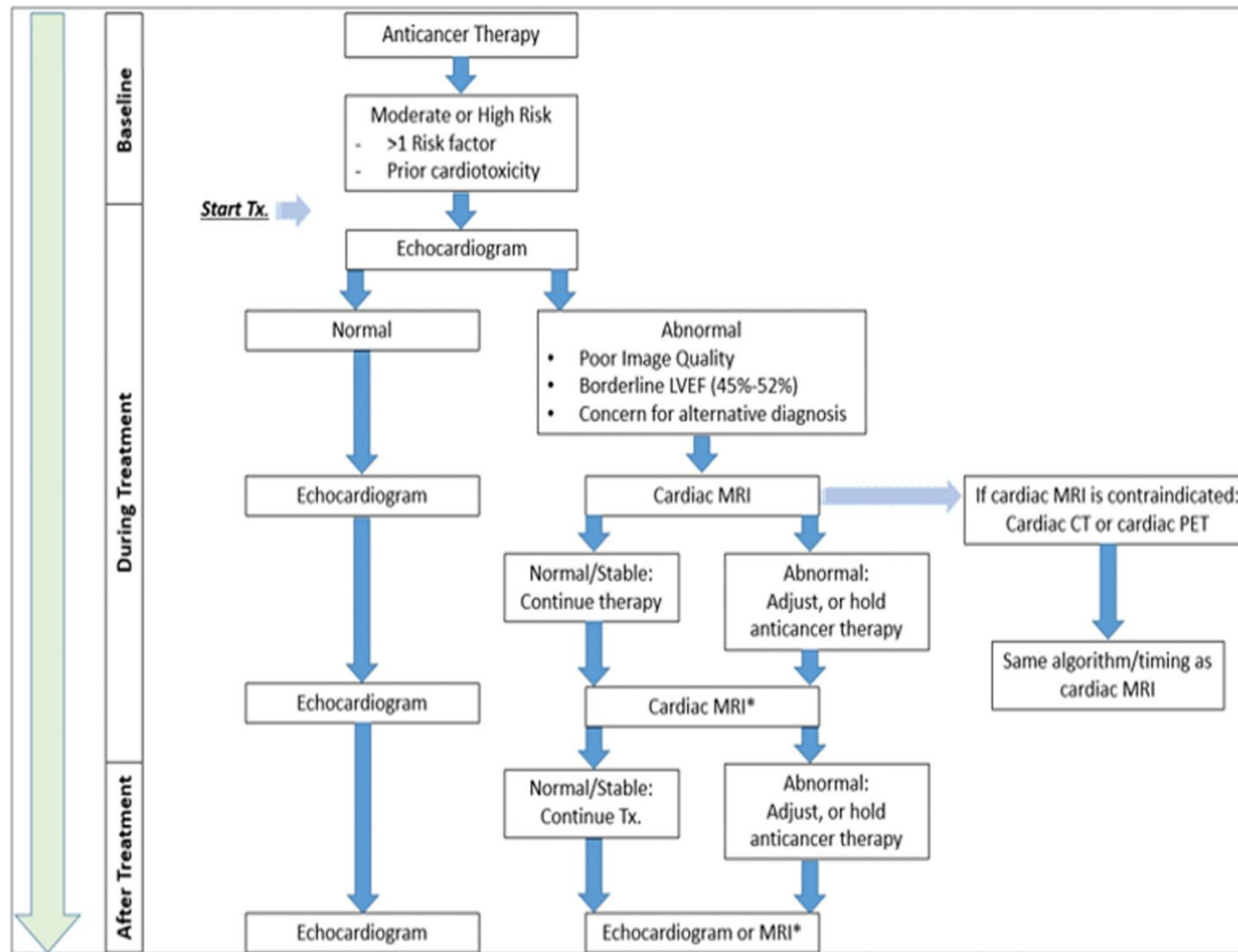
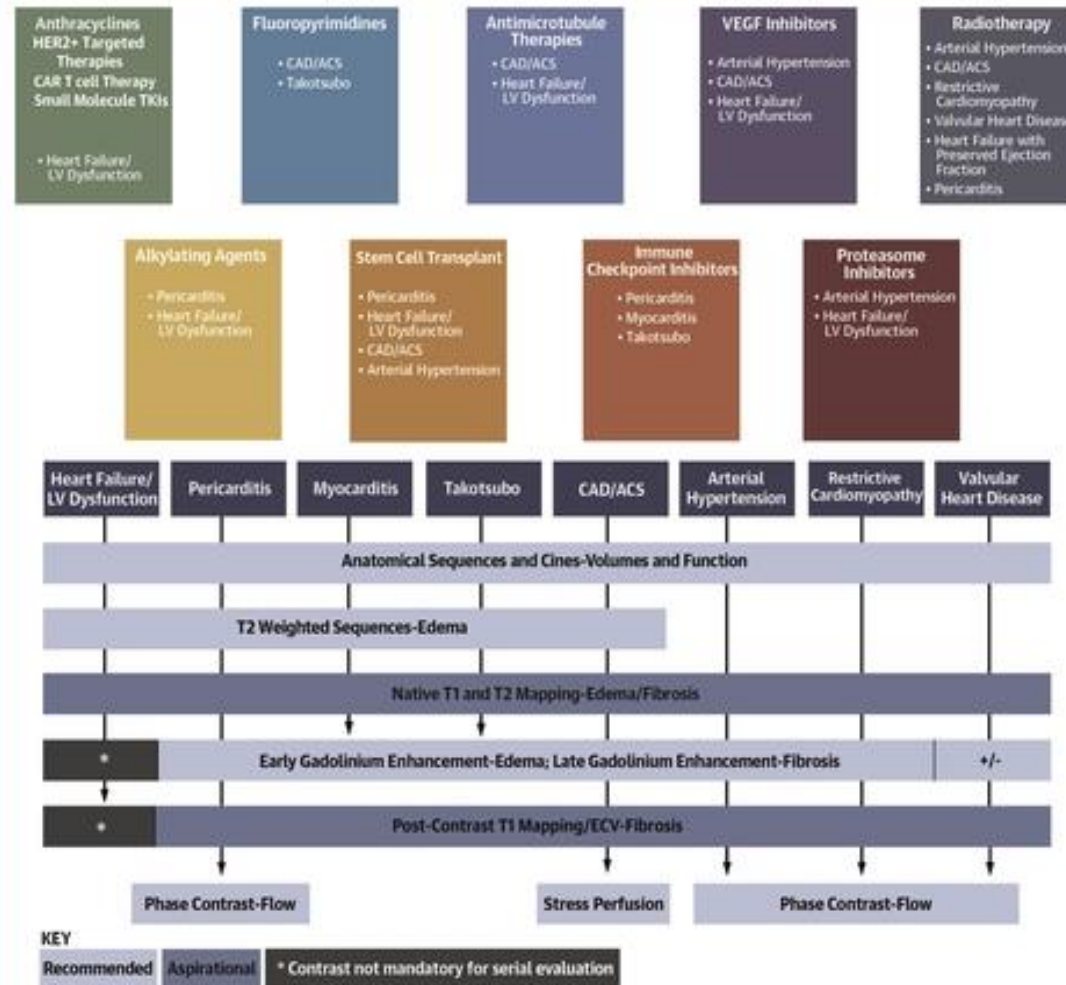


Figure 2. Suggested algorithm for monitoring left ventricular function before, during, and after cancer therapy for function monitoring.\* CT indicates computed tomography; LVEF, left ventricular ejection fraction; MRI, magnetic resonance imaging; PET, positron emission tomography; and Tx, treatment. **Risk factors include (but are not limited to) age >50 years, hypertension, diabetes, cardiac arrhythmia, and prior heart failure.** \*Additional imaging during treatment should be tailored to the patient's cardiotoxic risk profile and treatment. **All patients initiating anthracycline and HER2 therapies should have a baseline LVEF assessment as part of risk stratification.**



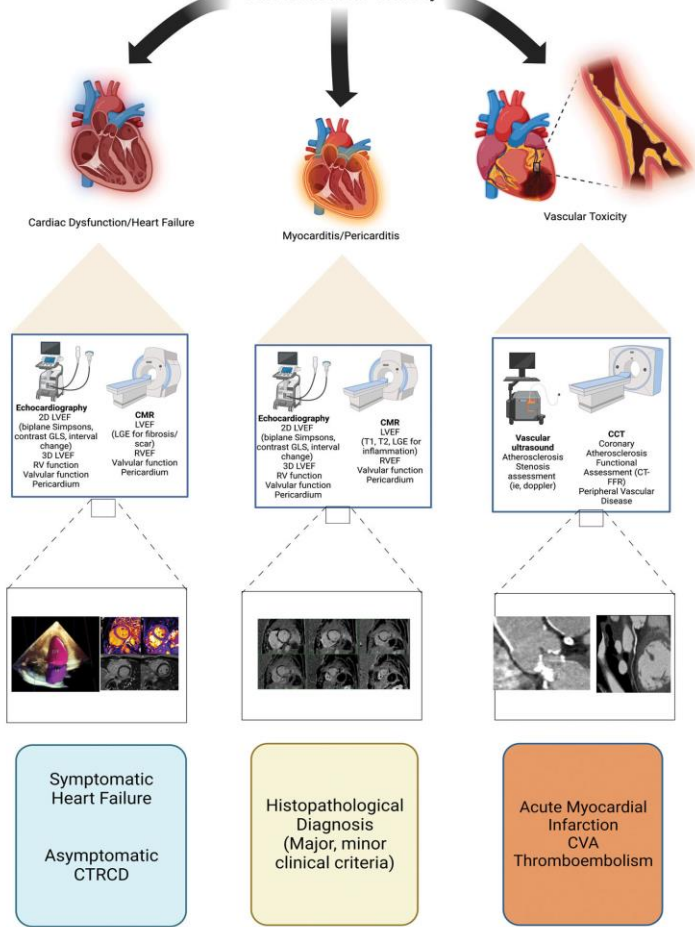
## CENTRAL ILLUSTRATION: Typical Cardiovascular Effects of Classes of Cancer Therapy With Suggested Cardiovascular Magnetic Resonance Imaging Protocols



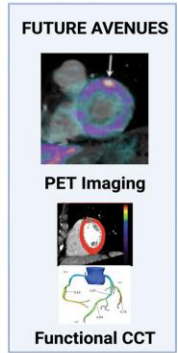
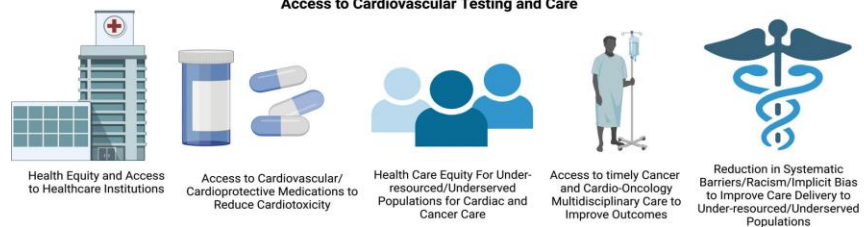
Harries, I. et al. *J Am Coll Cardiol CardioOnc.* 2020;2(2):270-92.

Iwan Harries et al. *J Am Coll Cardiol CardioOnc* 2020; 2:270-292.

# Multimodality Imaging Applications in Cancer Treatment-Associated Cardiovascular Toxicity



## Identification of Health Disparities and Gaps in Access to Cardiovascular Testing and Care



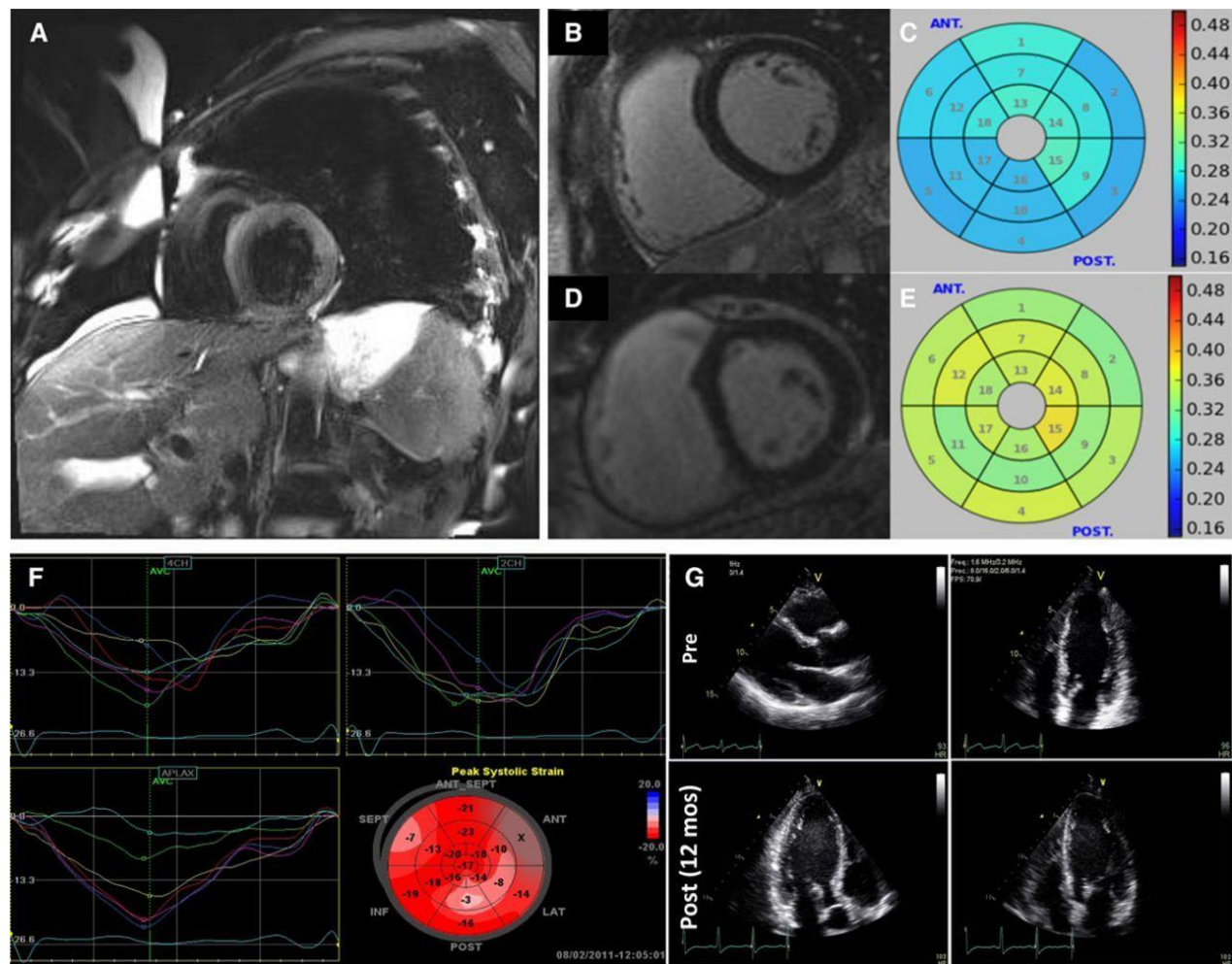
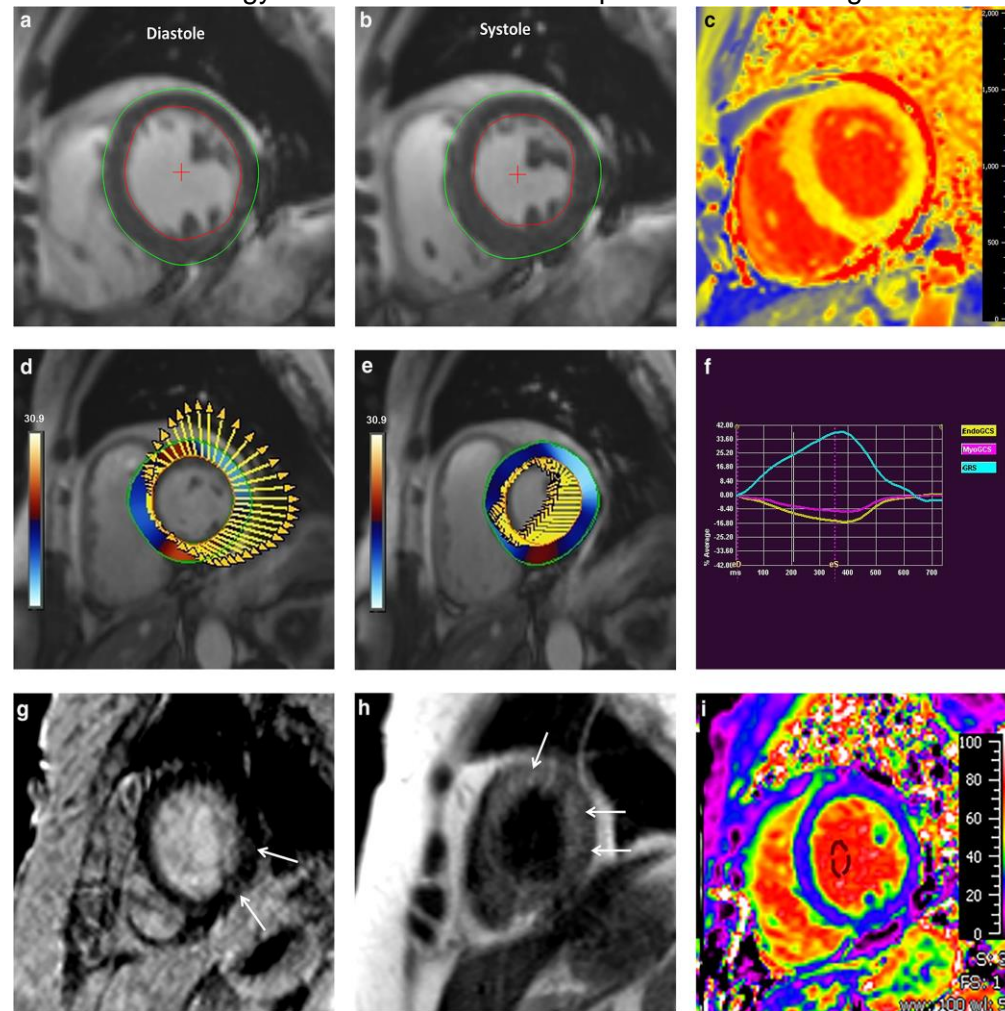


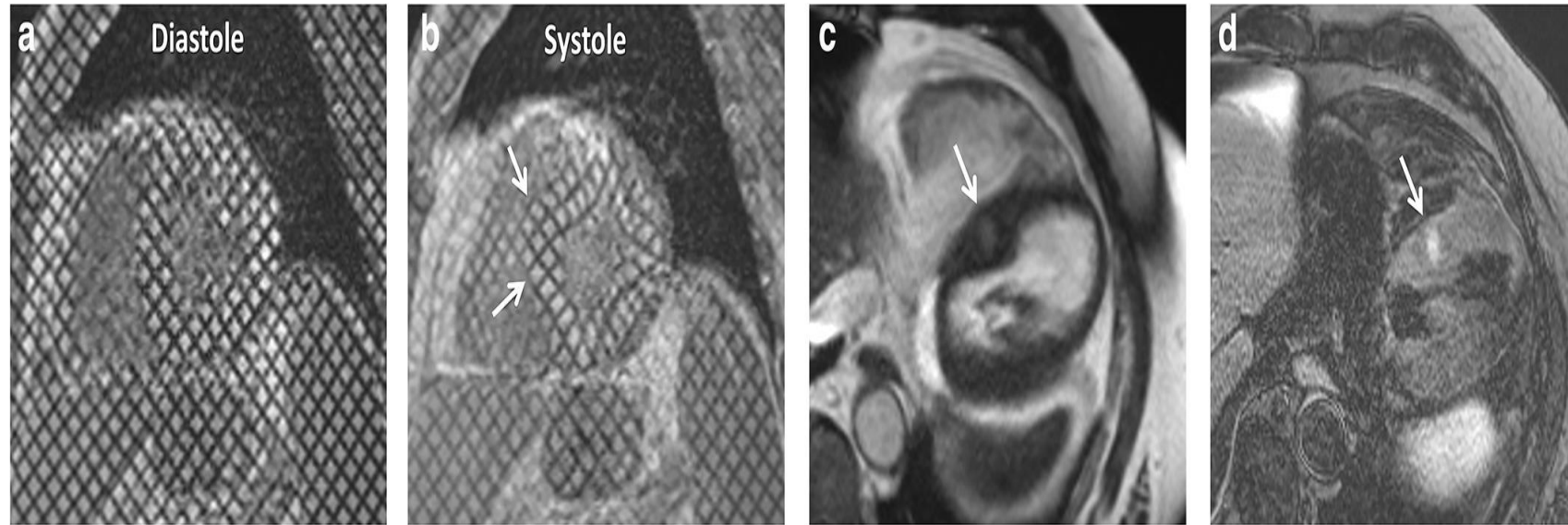
Figure 4. Multimodality imaging in early detection of cardiac toxicity from cancer therapy. A, Black blood short-axis CMR image showing elevated T2 signal consistent with myocardial inflammation in several segments of the LV in a patient who started anthracycline-based chemotherapy several days before and presented with palpitations and a minimally elevated cardiac troponin. B and C, Contrast CMR short-axis images from a healthy control (B) and a patient who had anthracycline therapy for sarcoma 6 years before imaging (C) demonstrating no evidence of LGE. However, the extracellular volume from T1 measurements demonstrate a higher extracellular volume of 0.35 in the anthracycline-treated patient in comparison with a volume of 0.26 in the healthy control. (Images in A through E are courtesy of Dr Tomas Neilan, Massachusetts General Hospital, Boston, MA.) F and G, 2D echocardiographic images of a patient with breast cancer obtained before and after chemotherapy. There was normal LVEF prechemotherapy and 12 months after chemotherapy. Global longitudinal strain was normal at baseline but reduced 3 months after chemotherapy (images courtesy of Dr Thomas Marwick)



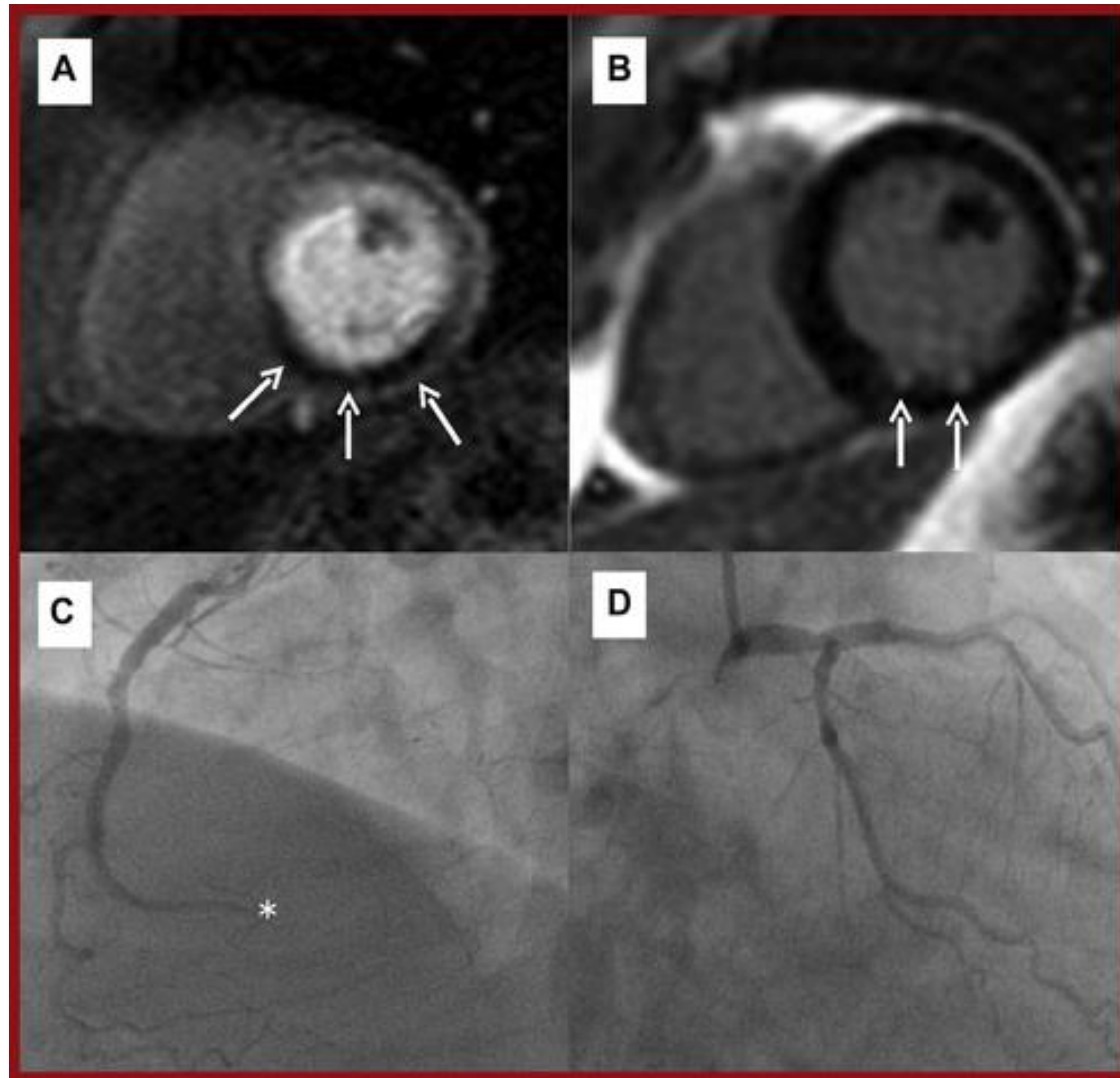
## MRI in cardio-oncology: A review of cardiac complications in oncologic care



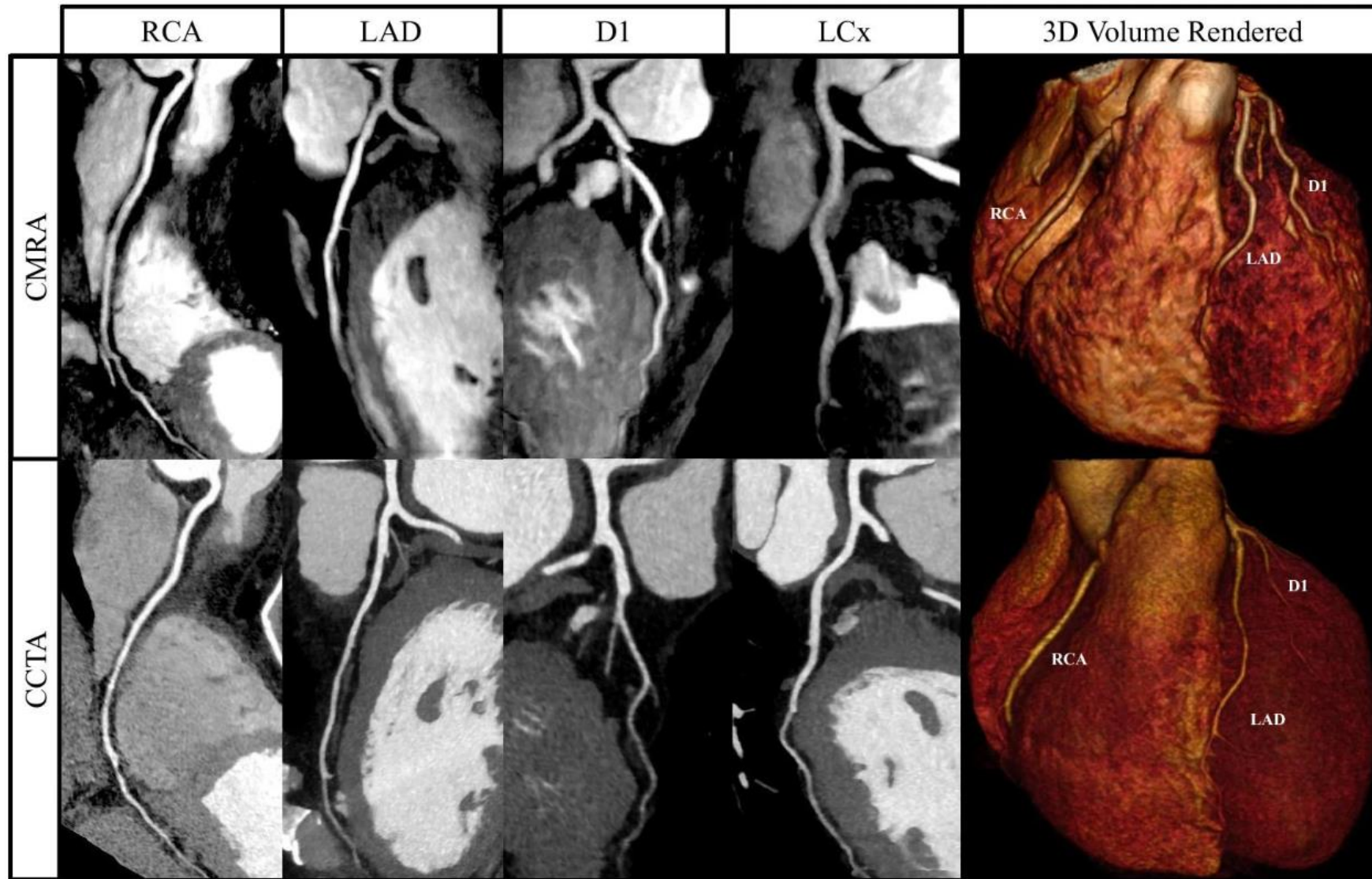
A 72-year-old female on therapy for diffuse large B-cell lymphoma. Diastolic (a) and systolic (b) short-axis bSSFP images with epicardial (green) and endocardial (red) tracings. LVEF was decreased to 35%. (c) Short-axis native T1 map color image shows elevated T1 relaxation times of 1110 msec in the anterior wall. Endocardial peak velocity vectors are shown in LV relaxation (d) and contraction (e) phases as yellow arrows. (f) Graphic representation of global strain throughout the cardiac cycle: endocardial global circumferential strain (yellow line), myocardial global circumferential strain (purple line), and global radial strain (light blue line). Myocardial global circumferential strain was -9.0 and global radial strain was 39%, both are abnormally decreased based on Ref. . (g) Short-axis postgadolinium phase sensitive inversion recovery image shows subtle mid-myocardial late gadolinium enhancement in the inferior and lateral LV walls suggesting fibrosis. (h) Short-axis double inversion recovery image shows patchy increased T2-weighted signal in the lateral and anterior LV walls compatible with edema. (i) Short-axis ECV image processed with Qmap software (Medis) shows increased ECV in the inferior wall of 33.6%. Findings were compatible with acute myocarditis. This patient suffered morbidity from disease relapse and therapy side effects and had died within 1 month following this MRI evaluation. Significantly decreased LVEF can be a late finding in the evaluation for cardiotoxicity with oncologic therapies.



An 81-year-old male with abnormal LV myocardial deformation related to interventricular septum metastasis from small bowel carcinoid tumor. (a) Diastolic and (b) systolic tagged images show the selective RF pulse-induced grid pattern which sticks with the myocardium during the cardiac cycle. Normal myocardial deformation during systole is seen in the anterolateral and inferior walls. Abnormal decreased contractility is noted by grid boxes which do not deform during systole (arrows). These short-axis images are located basal to the interventricular metastasis. (c) Axial bSSFP image shows a hyperintense mass in the interventricular septum with focal myocardial thickening (arrow). (d) Axial T2-weighted SPAIR image shows high T2-weighted signal within the mass (arrow). In this case, the abnormal contractility is related to a nearby ventricular metastasis. However, abnormal myocardial strain is more commonly seen with myocarditis and cardiomyopathies. Quantification of the abnormal deformation of the tagged grid represents the basis for the earliest myocardial strain measurements.

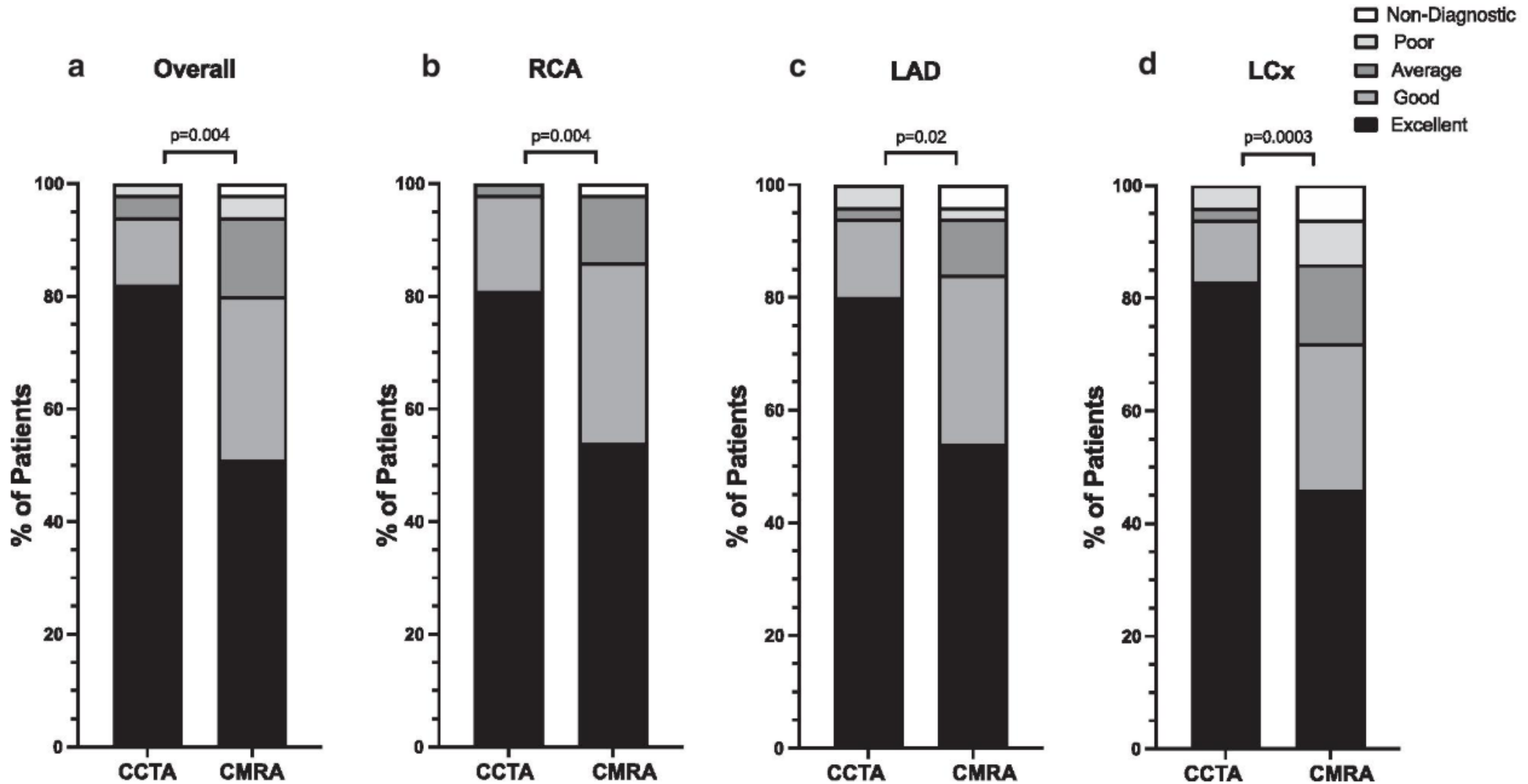


From: [Clinical comparison of sub-mm high-resolution non-contrast coronary CMR angiography against coronary CT angiography in patients with low-intermediate risk of coronary artery disease: a single center trial](#)



Curved multiplanar reformat and 3D volume rendered non-contrast coronary CMRA and contrast enhanced coronary CTA in a 54 year old male with no significant stenosis. D1-First diagonal coronary artery

From: [Clinical comparison of sub-mm high-resolution non-contrast coronary CMR angiography against coronary CT angiography in patients with low-intermediate risk of coronary artery disease: a single center trial](#)



Distribution of image quality scores for coronary CTA vs. coronary CMRA. **a** The overall 3D whole-heart dataset, **b** RCA, **c** LAD and **d** LCx

## Table 2 Diagnostic performance of 3D whole-heart coronary CMRA compared with coronary CTA

From: [Clinical comparison of sub-mm high-resolution non-contrast coronary CMR angiography against coronary CT angiography in patients with low-intermediate risk of coronary artery disease: a single center trial](#)

	Sensitivity	Specificity	PPV	NPV	Accuracy
<b>Per Patient</b>	<b>100 (12/12) [76–100]</b>	<b>74 (28/38) [58–85]</b>	<b>55 (12/22) [35–73]</b>	<b>100 (28/28) [88–100]</b>	<b>80 (40/50) [67–89]</b>
<b>Per Vessel</b>	<b>81 (13/16) [57–93]</b>	<b>88 (115/130) [82–93]</b>	<b>46 (13/28) [30–64]</b>	<b>97 (115/118) [93–99]</b>	<b>88 (128/146) [81–92]</b>
RCA	60 (3/5) [23–93]	91 (41/45) [79–96]	43 (3/7) [16–75]	95 (41/43) [85–99]	88 (44/50) [76–94]
LAD	88 (7/8) [53–99]	86 (36/42) [72–93]	54 (7/13) [29–77]	97 (36/37) [86–100]	86 (43/50) [74–93]
LCx	100 (3/3) [44–100]	91 (39/43) [78–96]	43 (3/7) [16–75]	100 (39/39) [91–100]	91 (42/46) [80–97]
<b>LM</b>	<b>N/A (0/0)</b>	<b>98 (49/50) [90–100]</b>	<b>0 (0/1) [0–95]</b>	<b>100 (49/49) [93–100]</b>	<b>98 (49/50) [90–100]</b>
<b>Per Segment</b>	<b>76 (16/21) [55–89]</b>	<b>95 (378/398) [92–97]</b>	<b>44 (16/36) [30–60]</b>	<b>99 (378/383) [97–99]</b>	<b>94 (394/419) [91–96]</b>
Proximal	70 (7/10) [40–89]	95 (173/182) [91–97]	44 (7/16) [23–67]	98 (173/176) [95–99]	94 (180/192) [89–96]
Middle	100 (6/6) [61–100]	92 (82/89) [85–96]	46 (6/13) [23–71]	100 (82/82) [95–100]	93 (88/95) [86–96]
Distal	60 (3/5) [23–93]	97 (123/127) [92–99]	43 (3/7) [16–75]	98 (123/125) [94–100]	95 (126/132) [90–98]

Significant values are indicated in bold

% (raw data) [95% confidence interval]

RCA, Right coronary artery; LAD, Left anterior descending coronary artery; LCx, Left circumflex coronary artery; LM, Left main coronary artery; PPV, Positive predictive value; NPV, Negative predictive value

## Graphical Abstract

### 4D flow CMR Clinical and Investigational Clinical Applications

#### Based on conventional flow velocity parameters

##### Atrial flow characteristics in AF patients

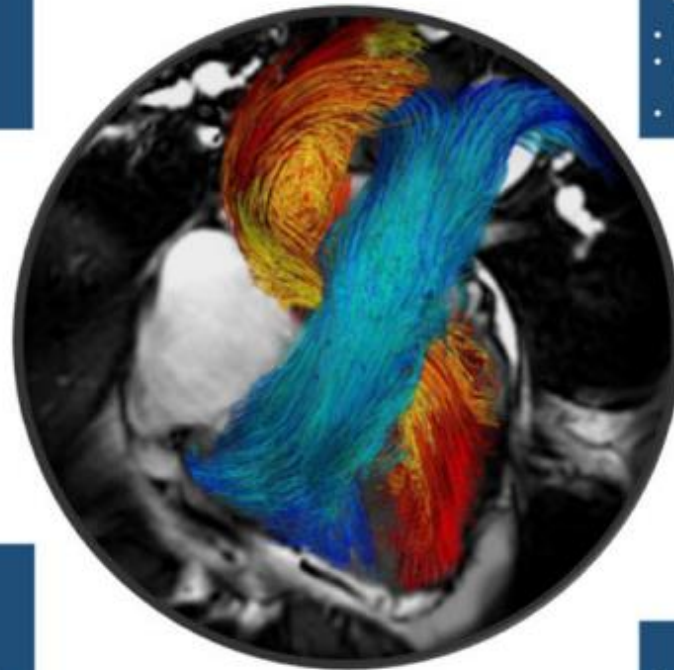
- Visual evaluation of 3D flow patterns in LA
- Quantification of global mean/peak flow velocity in LA
- Quantification of stasis fraction in LA (based on pre-determined cut-off values)

##### Valvular disease

- Retrospective direct quantification of valvular regurgitation for all cardiac valves with correct through plane placements
- Application of retrospective valvular tracking for a reproducible and accurate transvalvular flow quantification
- Retrospective peak velocity quantification of stenotic jets (particularly for eccentric and multiple jets)

##### Congenital heart diseases

- Easy planning of a single 3D volume acquisition
- Retrospective analysis at any location in 3D acquisition volume
- Internal control of balance between Qp and Qs (data quality check and rule in/out of shunts)
- Advanced visual evaluation of 3D flow patterns in the vicinity of surgically changed heart structures



#### Based on novel hemodynamic parameters

##### Clinical index in LV systolic/diastolic dysfunction patients

- Decreased LV KE over the whole cardiac cycle after MI
- Reduced LV KE at end-diastole in heart failure patients with mild LV remodelling
- Increased LV TKE at late diastole in DCM patients

##### Classification of LV filling

- Strong relation between LV KE during E/A waves and increasing age

##### Management of valvular disease

- Increased TKE in ascending aorta in patients with aortic valve stenosis
- Significant relation between LA TKE and regurgitant volume in patients with mitral regurgitation

##### Management of post-valvular intervention

- Impaired recovery of flow energy profiles after mitral valve intervention for mitral valve insufficiency

##### Index for quantification of LV dyssynchrony

- Altered intra-cardiac pressure maps and hemodynamic forces in patients with left ventricular dyssynchrony

##### Clinical index in congenital heart diseases

- Increased LV EL during diastole in corrected AVSD patients

## Keywords

4D flow cardiovascular MRI • clinical • flow • velocity • kinetic energy

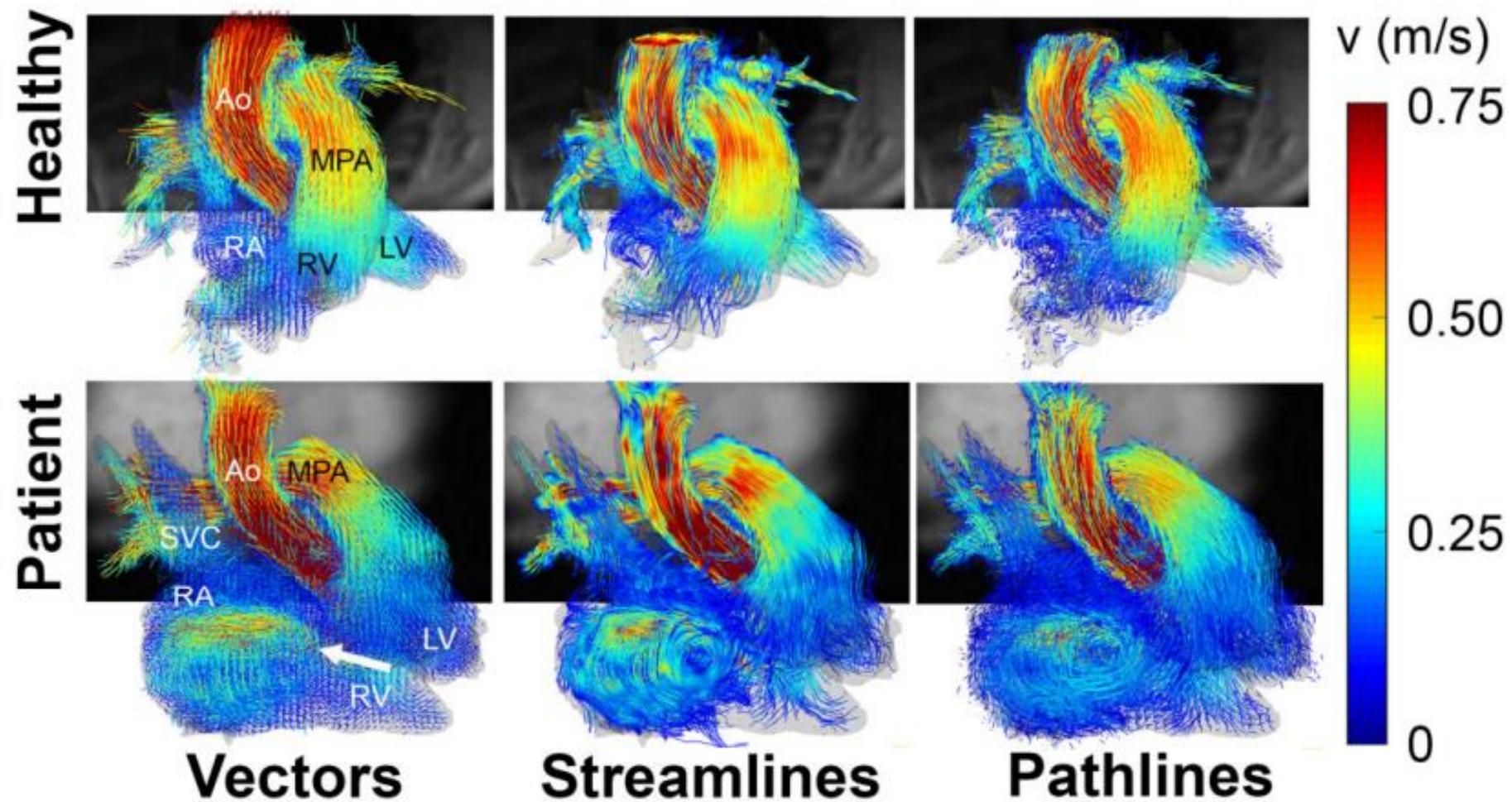


**Figure 1** 3D blood flow visualization with 4D flow CMR. 3D blood flow visualization on the whole heart is shown during mid-systole in a 28-year-old healthy male (top) and a 52-year-old female patient with tricuspid regurgitation (white arrow) after ventricular septal defect repair. Vectors, streamlines, and pathlines are illustrated from left to the right. Ao, aorta; MPA, main pulmonary artery; RA, right atrium; SVC, superior vena cava.

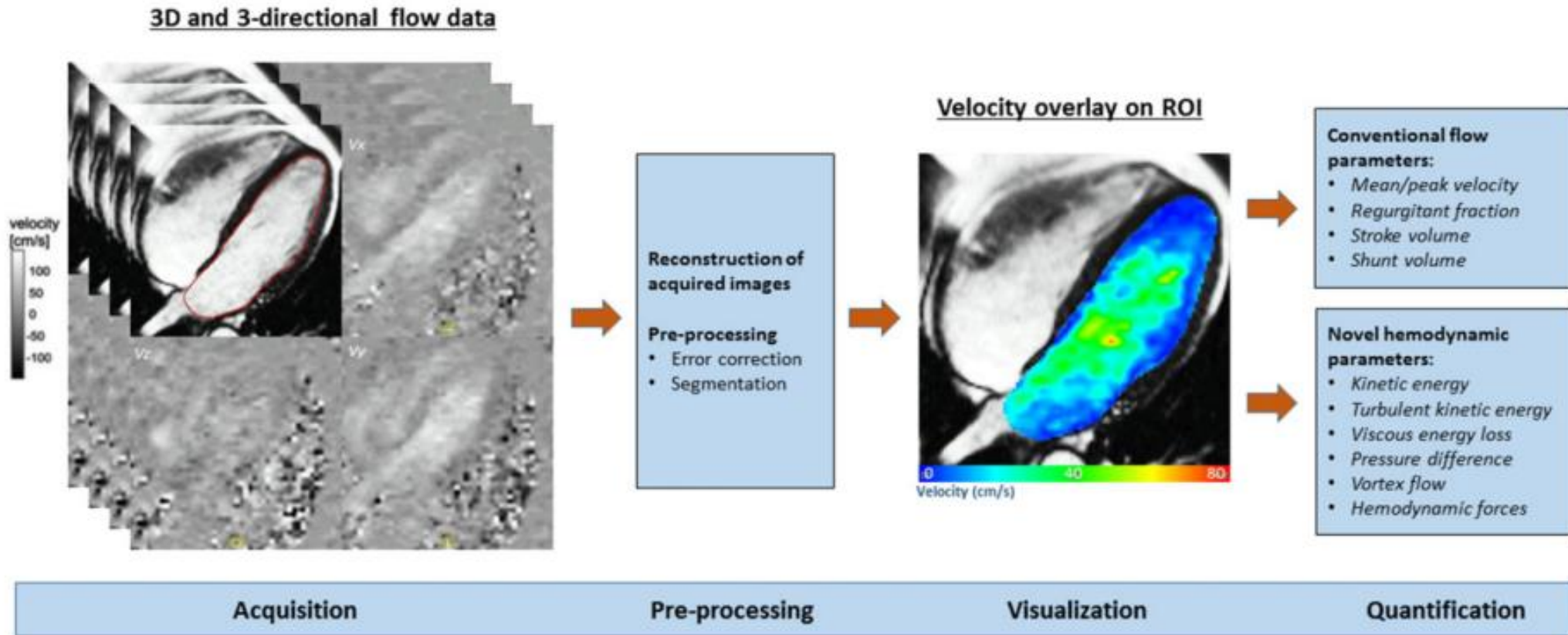
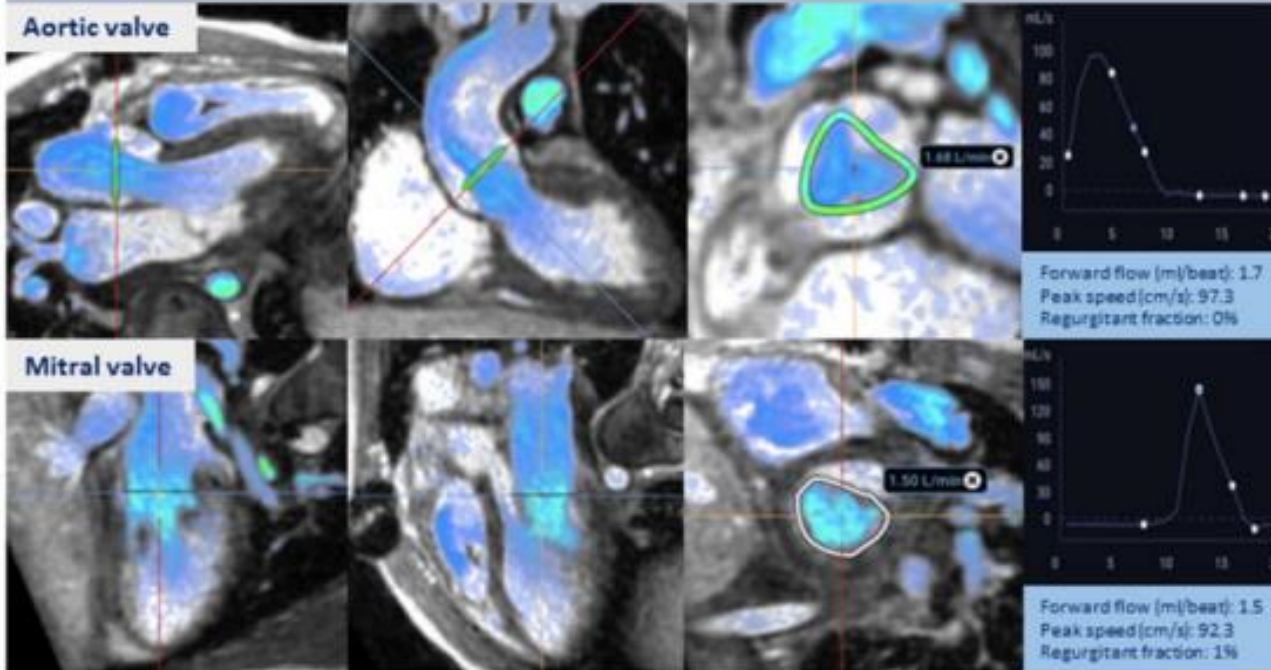


**Figure 2** Overview of 4D flow CMR acquisition and analysis process. A typical workflow for 4D flow CMR data acquisition and analysis is demonstrated using images of a healthy volunteer (33-year-old male). On the left side, the acquisition of images in 3-direction ( $x, y, z$ ) in a 3-dimensional volume of interest is displayed through flow velocity and magnitude images. Thereafter, acquired images are reconstructed and sequence-specific errors are corrected either manually or automatically. The segmentation is performed to determine the region of interest for visualization and quantification. In the middle-right, velocity overlay on the left ventricle and atrium during early diastole was illustrated. On the right side, conventional and novel hemodynamic parameters which can be generated through 4D flow CMR data are displayed. ROI, region of interest.

## 4D flow CMR



## 4D color Doppler echocardiography

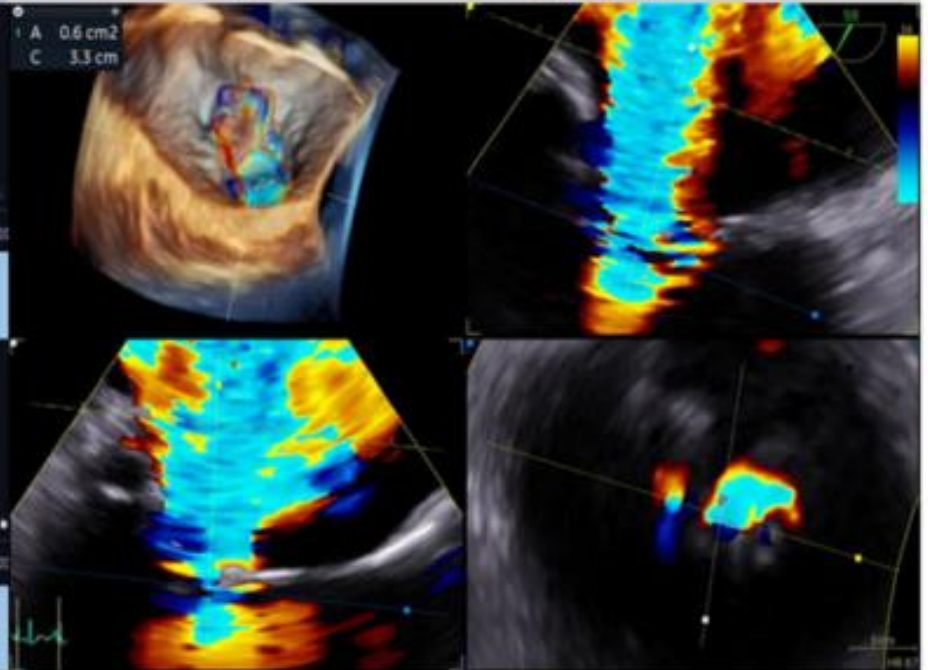


**Figure 7** Valvular flow quantification with 4D flow CMR and 4D colour Doppler echocardiography. On the left side, valvular flow visualization and quantification of 4D flow CMR is displayed in a 12-year-old healthy male. 3D blood flow on multi-planar views during systole for aortic valve and during diastole for mitral valve is visualized. The segmentations were done using an artificial intelligence approach. Furthermore, aortic and mitral valve flows are temporally plotted over the cardiac cycle and valvular flow measurements are provided. On the right side, measurement of 3D vena contracta area of functional mitral regurgitation with 4D colour Doppler transesophageal echocardiography in a 51-year-old male is shown. Volume rendering view (top left), two perpendicular long-axis views of mitral regurgitation jet and one short-axis view (bottom right) at the level of coaptation defect are visualized. Vena contracta area was measured as 0.6 cm<sup>2</sup> and circumference of the jet as 3.3 cm.

# Conclusion

- ▶ Imaging is complimentary
- ▶ Software and hardware advancements have accelerated tremendously
- ▶ AI continues to advance make patient care better and more efficient
- ▶ The future is looking bright in cardiovascular imaging

# References

- ▶ 1. Medvedofsky D et al. Three dimensional echocardiographic quantification of the left-heart chambers using an automated adaptive analytics algorithm: multicenter validation study. *European Heart Journal-Cardiovascular Imaging*, Volume 19, Issue 1, January 2018, Pages 47-58.
- ▶ 2. Papadopoulos K et al. Initial Experience with the 4D Mini-TEE Probe in the Adult Population. *J. Clin. Med.* 2024, 13, 6450.
- ▶ 3. Sagit Ben Zekry. *Circulation: Cardiovascular Imaging*. Patient-Specific Quantitation of Mitral Valve Strain by Computer Analysis of Three-Dimensional Echocardiography, Volume: 9, Issue: 1, DOI: (10.1161/CIRCIMAGING.115.003254)
- ▶ 4. Ruberg FL and Maurer MS. Cardiac Amyloidosis Due to Transthyretin Protein: A Review. *JAMA*. 2024;331(9):778-791
- ▶ 5. Marcelo F. Di Carli. *Circulation*. The Future of Cardiovascular Imaging, Volume: 133, Issue: 25, Pages: 2640-2661, DOI: (10.1161/CIRCULATIONAHA.116.023511)
- ▶ 6. Tom Kai Ming Wang. *Circulation: Cardiovascular Imaging*. Diagnosis of Infective Endocarditis by Subtype Using 18F-Fluorodeoxyglucose Positron Emission Tomography/Computed Tomography, Volume: 13, Issue: 6, DOI: (10.1161/CIRCIMAGING.120.010600)
- ▶ 7. Marc R. Dweck. *Circulation: Cardiovascular Imaging*. 18F-Sodium Fluoride Uptake Is a Marker of Active Calcification and Disease Progression in Patients With Aortic Stenosis, Volume: 7, Issue: 2, Pages: 371-378, DOI: (10.1161/CIRCIMAGING.113.001508)
- ▶ 8. Martha Gulati. *Circulation*. 2021 AHA/ACC/ASE/CHEST/SAEM/SCCT/SCMR Guideline for the Evaluation and Diagnosis of Chest Pain: A Report of the American College of Cardiology/American Heart Association Joint Committee on Clinical Practice Guidelines, Volume: 144, Issue: 22, Pages: e368-e454, DOI: (10.1161/CIR.0000000000001029)
- ▶ 9. Charalambos Antoniades, Henry W West, Coronary CT angiography as an 'one-stop shop' to detect the high-risk plaque and the vulnerable patient, *European Heart Journal*, Volume 42, Issue 37, 1 October 2021, Pages 3853-3855
- ▶ 10. Dodd JD and Leipsic JA. Evolving Developments in Cardiac CT. *Radiology* 2023; 307(3):e222827
- ▶ 11. Daniel Addison. *Circulation*. Cardiovascular Imaging in Contemporary Cardio-Oncology: A Scientific Statement From the American Heart Association, Volume: 148, Issue: 16, Pages: 1271-1286, DOI: (10.1161/CIR.0000000000001174)
- ▶ 12. Harries, I, Liang, K, Williams, M. et al. Magnetic Resonance Imaging to Detect Cardiovascular Effects of Cancer Therapy: *JACC CardioOncology* State-of-the-Art Review. *J Am Coll Cardiol CardioOnc*. 2020 Jun, 2 (2) 270-292.
- ▶ 13. Jeong D, et al. MRI in Cardio-oncology: A Review of Cardiac Complications in Oncologic Care. *J. MAGN. RESON. IMAGING* 2019;50:1349-1366.
- ▶ 14. Hajhosseiny R et al. Clinical comparison of sub-mm high-resolution non-contrast coronary CMR angiography against coronary angiography in patients with low-intermediate risk of coronary artery disease: a single center trial. *Journal of Cardiovascular Magnetic Resonance* 23, Article number: 57 (2021)
- ▶ 15. Demirkiran A et al. Clinical intra-cardiac 4D flow CMR: acquisition, analysis, and clinical applications. *European Heart Journal-Cardiovascular Imaging* (2022) 23, 154-165.